Hopkinson bar experimental technique: A critical review

Bazle A Gama

Department of Materials Science and Engineering, University of Delaware–Center for Composite Materials (UD-CCM), Newark DE 19716; gama@ccm.udel.edu

Sergey L Lopatnikov

Department of Civil and Environmental Engineering, University of Delaware–Center for Composite Materials (UD-CCM), Newark DE 19716; lopatnik@ccm.udel.edu

John W Gillespie Jr

Department of Materials Science and Engineering, Department of Civil and Environmental Engineering, University of Delaware–Center for Composite Materials (UD-CCM), Newark DE 19716; gillespie@ccm.udel.edu

A critical review of three classic papers by B Hopkinson, RM Davies, and H Kolsky, and the state-of-the-art in Hopkinson bar experimental techniques is presented. The validity and applicability of the assumption made in the 1D Hopkinson bar theory are discussed. Fundamentals of the Hopkinson bar experimental procedure are outlined including bar calibration, specimen design, pulse shaping, and data analysis following the essential dispersion correction methodology. Additional data tables necessary for dispersion correction are provided to cover a wide range of Poisson's ratio. In addition to the elastic-plastic metals, methodologies for soft and hard materials are also discussed. This paper provides the necessary information for conducting a Hopkinson bar experiment and analyzing the experimental data. This review article cites 61 references. [DOI: 10.1115/1.1704626]

INTRODUCTION

The history of the development and theory of the Hopkinson Bar for high strain rate testing of materials is presented in this paper. The Hopkinson bar experimental technique evolved as a consequence of stress wave experiments in iron wires performed by John Hopkinson (1872) [1,2] and later experiments by his son Bertram Hopkinson (1905) [3]. A decade later, B Hopkinson (1914) developed the famous *pressure bar* technique to experimentally determine the pressure produced by an explosive [4]. About 34 years later, RM Davies (1948) used electrical condenser units in conjunction with oscilloscopes to record the wave propagation in the *pressure bar* for the first time [5]. The following year H Kolsky (1949) used the *pressure bar* technique in determining the dynamic compression stress-strain behavior of different materials [6] by increasing the length of the *time piece* of the *pressure bar* and using the *time piece* as an *extension bar*. These classic studies have established the foundation for the state-of-the-art experimental methods and data analysis technique, and are critically reviewed.

Davies [5] published a critical review of Hopkinson's [4] original work and discussed the limitations and dispersion effects in the *pressure bar* technique. Kolsky [6] developed the 1D *pressure bar* data analysis technique and the experimental procedure. This history of Hopkinson Bar development and some remarks on the classic papers are presented in the following section, Historical Background. Scientists and engineers have widely used Kolsky's [6] original compression *pressure bar* technique in characterizing the high-strain rate behavior of engineering materials. In the 20th century, the use of the Hopkinson Bar technique has been extended to accommodate tension, shear, torsion, bending, indentation, and combined load cases. The state-of-the-art in Hopkinson Bar technique is summarized in the section, Recent Advances in Hopkinson Bar Experimental Techniques. The components of a Hopkinson Bar apparatus, its operating principles, traditional 1D stress wave analysis, and assumptions of a valid test are summarized in the section, Components of Split-Hopkinson Pressure Bar and 1D Data Analysis. It is well known from the work of Davies [5] that the Hopkinson Bar technique and its 1D assumption have several limitations and is discussed in the section, A Critical Analysis of Traditional 1D Stress Wave Theory of SHPB. A successful Hopkinson Bar experiment should follow a carefully designed experiment, which includes the calibration of the equipment, specimen design to minimize friction, inertia effects, and stress nonequilibrium of the specimen. Specimen

Transmitted by Associate Editor J. Engelbrecht

design with materials other than elastic-plastic metals such as polymers, rubbers, foamed materials, composites, and ceramics requires additional consideration and diagnostics. These issues are discussed in the section, General Guidelines for SHPB Testing.

The 1D time domain theory of Hopkinson Bar experimental techniques appear to be rather simple. However, the dispersion effect present in a finite diameter bar suggests that the dispersion correction be performed in frequency domain. A data reduction methodology in frequency domain incorporating dispersion correction and delay setting is presented in the section, Data Processing and Dispersion Correction in SHPB Testing. This review presents a complete history and addresses throughout the 20th century to present day advances in Hopkinson Bar techniques. The traditional 1D stress wave theory of Hopkinson Bar and the associated assumptions are outlined. A critical analysis of the validity and applicability of the 1D theory are presented. A general guideline for Hopkinson Bar testing, and the detail data-processing methodologies in the frequency domain are described. There are 61 references in this review article selected for their significant contribution to this field of high strain-rate testing.

HISTORICAL BACKGROUND

In 1872, J Hopkinson [1,2] published two papers in the *Proceedings of the Manchester Literary and Philosophical Society* on the rupture of iron wire by a blow. These papers describe the theory of a propagating wave through an iron wire fixed at one end while the other end is suddenly loaded under tension by the impulse produced by a moving mass, and presents the experimental results of the strength of iron wires under different loading conditions. The loading conditions, by the appropriate choice of mass and velocity of the falling body, were used as parameters to investigate whether the rupture of the iron wire takes place near the impulse end (direct wave) or near the fixed end (reflected wave). It has been shown ''that half the velocity of impact needed to break the wire near the mass is sufficient to break it at the fixed point.''

Following the pioneering work of J Hopkinson [1,2], about 33 years later, B Hopkinson [3] revisited his father's work and formulated analytical expressions for the total increase in length of an impulsively loaded wire, which is fixed at one end. He designed an experiment to measure the momentary extension through a contact device and a ballistic galvanometer. In this experiment, a contact device is placed at a predetermined distance; contact or no-contact is identified from the galvanometer response. Multiple experiments were necessary to determine the correct extension, however, it is probably the first work published in measuring the dynamic extension with state-of-the-art technology. The history of experimental techniques using the Hopkinson Bar starts with the pioneering work of B Hopkinson (1914) [4] followed by RM Davies (1948) [5], and H Kolsky (1949) [6]. The works of these three scientists are considered ''classics'' and are described in the following sections.

B Hopkinson [4]: The Pressure Bar

In 1914, B Hopkinson [4] developed an experimental procedure to measure the pressure produced by the impact of a bullet or by the detonation of gun cotton. This particular technique, which became well known as the *Hopkinson Pressure Bar* technique, is famous as a method in the dynamic characterization of materials. In this paper, Hopkinson observed that ''if a rifle bullet be fired against the end of a cylindrical steel rod there is a definite pressure applied on the end of the rod at each instant of time during the period of impact,'' essentially forming a pressure pulse. This impact induced pressure (compressive) pulse will propagate along the rod (B), and will reflect from the free end of the rod as a tension pulse. He also described how a small rod (C) of the same material and cross section would trap the momentum of the direct wave and fly off from the main pressure bar. The momentum of the flying *piece* (C) was measured by a ballistic pendulum (D) (Fig. 1). By measuring the maximum displacement and period, and knowing the mass of the ballistic pendulum, the momentum of the flying *piece* can easily be determined. Hopkinson showed that by varying the length of the momentum of the *piece*, the maximum amplitude of the pressure and the total duration could be measured; however, a perfect pressure pulse shape cannot be obtained.

The theory of wave dispersion in rods, as described by Love [7], was cited in this paper. Experiments were conducted with smaller bar lengths to study the effect of wave dispersion. It is very important to mention that the theory of 3D longitudinal stress wave propagation in an infinite cylindrical rod was developed by Pochhammer [8] and Chree [9]; and was known while Hopkinson [4] was conducting his

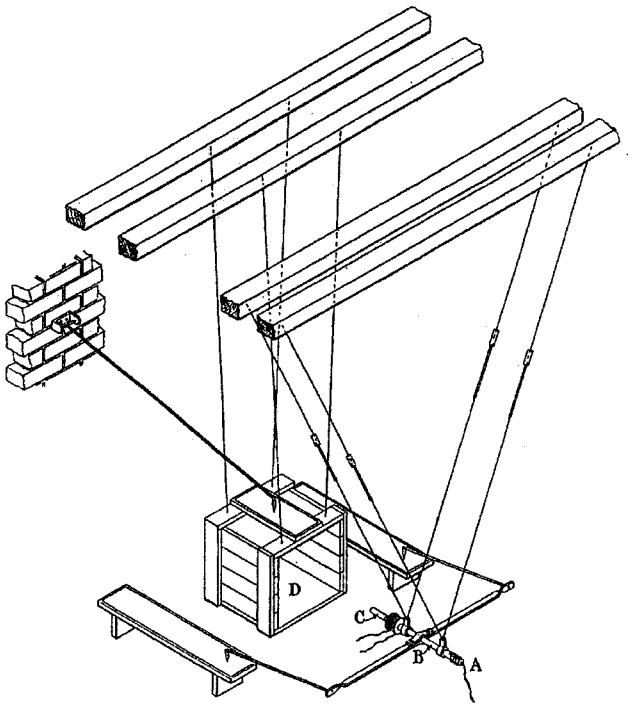

Fig. 1 Apparatus developed by Bertram Hopkinson for the measurement of pressure produced by the detonation of gun cotton. Reproduced from Fig. 12, Hopkinson [4], p 451.

experiments on the *Hopkinson Pressure Bar* in 1914. However, the momentum method of measurement showed an insignificant effect. In addition to the unique method developed, a wide parametric study of the effect of bar length and diameter, bullet types, gun cotton type, and explosion methods, and the use of a hard impact end on the pressure bar were described.

RM Davies [5]: A critical analysis of the Hopkinson Pressure Bar

About 34 years after Hopkinson [4] developed his Pressure Bar technique, Davies [5] presented the first dynamic axial and radial strain measurements in Hopkinson Pressure Bar experiments using parallel plate and cylindrical condensers in conjunction with a double beam cathode-ray oscillograph (Fig. 2). In addition to the new development in measurement techniques, Davies also discussed the limitations of the Hopkinson Pressure Bar experiment and measurement. ''Apart from any theoretical limitations associated with the distortion of a pressure pulse as it is propagated along a bar, the original Hopkinson method suffers from two disadvantages.'' The first disadvantage is that the magnetic adhesive force of the end-piece limits the minimum pressure that can be measured with accuracy. The second disadvantage is that the pressure-time history cannot be obtained.

Davies introduced the electrical measurement of the longitudinal displacement ξ of the bar end and the radial displacement ζ of the cylindrical surface of the bar as a function of time t. Considering the 1D elastic stress wave propagation in a bar with a free end, Davies showed that the bar end particle velocity and the radial displacement is related to the pressure in the bar p, by: $\dot{\xi}=2p/\rho c_0$ and $\zeta=\nu a p/E$ (Eqs. 1.2 and 1.3 in Davies [5]), where ρ is the density, c_0 is the bar wave velocity, ν is Poisson's ratio,[1] a is the radius of the bar, and E is Young's modulus. By measuring the displacements as a function of time, the pressure in the bar as a function of time can then be computed. Davies pointed out three major theoretical limitations of the original Hopkinson method, and the new electrical method ''arising from the assumptions which they are based and inherent in every method involving the propagation of a pulse along a bar of finite diameter.''

The three limitations as described by Davies can be summarized as:

1) the assumption of elastic wave propagation in the bar limits the pressure that can be measured by this technique
2) the assumption that the pressure pulse propagates without distortion is true only for long wavelengths as compared to the lateral dimension of the bar
3) the assumption that the pressure pulse is uniform over the crosssection is not true in the neighborhood of the pressure end

Davies performed similar experiments to Hopkinson [4]. Using Hopkinson's experimental setup Davies discussed several important issues: i) ''the material of the bar is homogenous and nowhere stressed beyond the limit of proportionality''; ii) the bar is ''uniform in diameter''; iii) ''the pressure end can be protected by an hard anvil of short length''; iv) ''slight smear of grease'' will hold the anvil; v) ''bars ranging in length from 2 to 22 ft. have been used''; vi) ''for most purposes, bars of diameter 0.5, 1 and 1.5 in. are suitable''; vii) the value of the longitudinal wave speed (also known as bar velocity) c_0 is determined by a dynamic vibration technique. The displacement as a function of time at the end of the bar, due to the pressure produced by the impact of a projectile at the impact end, was measured from the parallel plate condenser response (Fig. 3). The pressure is then calculated from the displacement rate using Eq. 1.2 from Davies [5]. Similarly, measuring the radial displacement as a function of time, the pressure-time response can also be obtained. Davies took the photograph of the condenser response from the cathode-ray oscilloscope, and took the measurement using a measuring microscope. The response of the cylindrical condensers gives the shape of the pressure (Fig. 4), while the response of the parallel plate condenser gives the shape of the displacement at bar end (Fig. 5).

Both these measurements show oscillations in the response. In order to make sure that his measurement is correct and the experimental error is minimal, Davies discussed the dispersion effects in the Hopkinson Bar using the general 3D solution of an infinite rod for sinusoidal longitudinal wave propagation loading as described by Pochhammer [6]. In contrast with the elementary/simple theory, Davies stated,

[1]Davies used the notation σ for Poisson's ratio

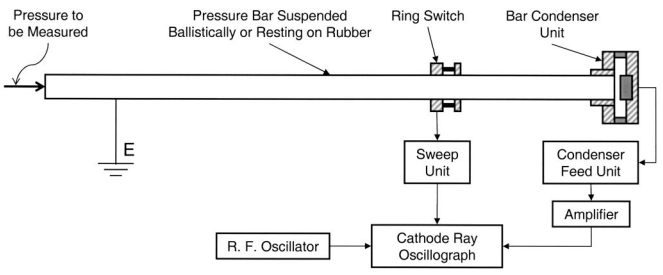

Fig. 2 General arrangement of the apparatus developed by Davies. Reproduced from Fig. 1, Davies [5], p 382.

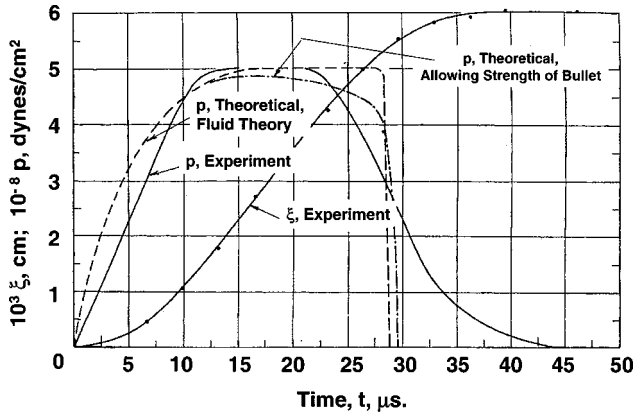

Fig. 3 Calculation of pressure in the Hopkinson Bar from displacement measurement at bar end. Reproduced from Fig. 12, Davies [5], p 403.

''According to the simple theory, the velocity of a sinusoidal wave is independent of Λ (wave length) and is equal to $c_0 = \sqrt{E/\rho}$; according to the general theory, c is determined by a, Λ, c_0, and ν, where (c/c_0) is a function of ν and (a/Λ), which is unity only in the limit when a/Λ is zero.'' Also, ''according to the simple theory, the longitudinal stress and displacement are uniform over the cross section of the bar, the radial stress is everywhere zero and the radial displacement at distance r from the axis is $\nu pr/E$. In general case, the longitudinal stress and displacement vary over the cross section of the bar, the radial stress is finite and the radial displacement does not follow the simple linear law.''

The solution of sinusoidal stress wave propagation in a finite diameter rod of infinite length can be found [8]. The nontrivial boundary conditions, which are zero traction on the surface of the finite diameter rod, yield the famous Pochhammer frequency equation. ''This equation has multiple roots, and solutions were found for the first three roots differing from zero, assuming $\nu = 0.29$,'' by Davies. A similar solution was also found by Bancroft [10] for the lowest nonzero roots of the frequency equation for values of ν ranging from zero to one half. The roots of the frequency equation can be expressed in a nondimensional form, which gives the dimensionless phase velocity c/c_0 as a function of a dimensionless wave number a/Λ. The first three nonzero roots are presented in Fig. 6.

Under the conditions which prevail in Hopkinson Bar experiments, it is unlikely that the second and third vibration modes are ever excited. The first mode of vibration is important, demonstrating that for long wavelengths $(a/\Lambda \to 0)$, the phase velocity approaches the value of bar velocity (c_0); and for short wavelengths $(a/\Lambda \to \infty)$, the phase velocity is less than the bar velocity and approaches the Raleigh surface wave velocity (c_S). A system is called *dispersive* if the phase velocity of a harmonic wave is a function of its wavelength. The Pochhammer frequency equation demonsrates that the elastic wave propagation in a finite diameter rod is *dispersive* in nature.

It is now well known that any longitudinal stress pulse generated at the impact end and propagating along the bar can be expressed as a sum of harmonic waves of different amplitudes and periods (experimental time data can be transformed into frequency domain using Fourier Transform). Generally, a sharp wave front contains high-frequency/short-wavelength harmonic waves, which will propagate slower than the low-frequency/long-wavelength waves. Consequently, the sharp wave front will smooth out, and high frequency oscillations will appear on the propagating pulse as the wave front propagates along the bar. A finite diameter Hopkinson Bar is thus a *dispersive* system and the net effect is that the width of an axial rectangular stress/pressure pulse propagating along the bar will increase, high frequency oscillations will appear, and the sharp fronts will be smoothed out. The pressure-time data obtained though the cylindrical condenser unit by Davies thus had ''obvious distortion of the main pulse'' and contains ''a train of high-frequency oscillations following the pulse. It is clearly impossible to derive an accurate (pressure, time) curve from these records'' (Fig. 4). The period or frequencies of the ''train of high frequency oscillation following the pulse'' can be measured from the experimental curves, and are essentially not the feature of the pressure pulse at the pressure end of the bar.

The displacement measured at the free end of the bar by Davies using a parallel plate condenser also contained dispersive effects (Fig. 5). This has also been verified using Love's approximate wave equation (Figs. 26 and 27 in Davies [5]). Generally, the dispersion has two effects: 1) ''The initial portions of the curves are not straight lines and they do not intersect the t-axis at a finite angle as they would do if dispersion is absent; instead, they are curved (concave upwards) and tangential to the t-axis. It should be pointed out that the curves begin to rise before the arrival of the wave of velocity c_0 at the measuring end of the bar''; 2) ''Beyond

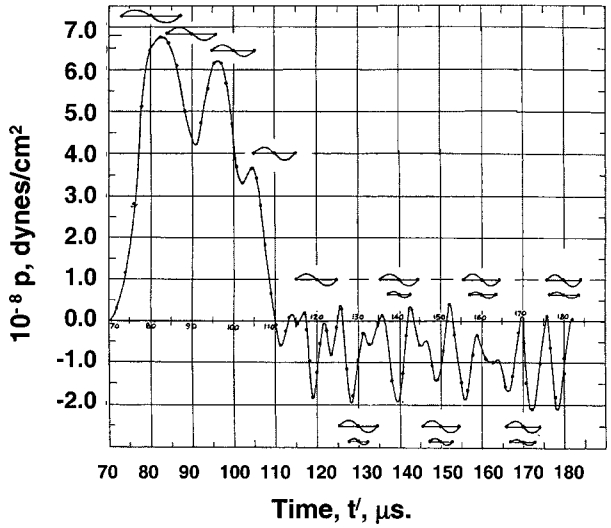

Fig. 4 Radial displacement data recorded and analyzed by Davies. Reproduced from Fig. 24, Davies [5], p 425.

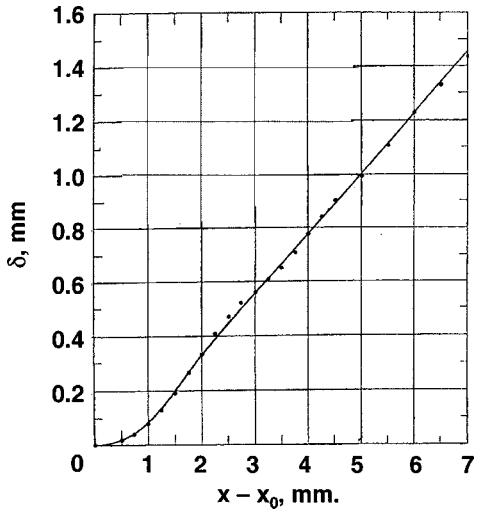

Fig. 5 Axial displacement data recorded and analyzed by Davies. Reproduced from Fig. 29, Davies [5], p 438.

their initial curved portions, the (ξ, t) curves oscillate, to varying degrees, about the straight lines which would be obtained with a distortion less bar.''

In addition to the discussion of distortions in his measurements using parallel and cylindrical condensers, Davies also calculated the distribution of dimensionless radial and axial displacements and stresses as a function of the dimensionless radius of the infinite rod subjected to harmonic wave loading using the equations as described in Love's book [7] for $\nu = 0.29$ and $a/\Lambda = 0.1968$ and 0.9355 (Fig. 7). These calculations show that the displacement and stress in the axial direction are nonplanar and in the radial direction are nonlinear.

In summary, Davies concluded:

1) The Pressure Bar is incapable of accurately measuring pressures that are subject to rapid changes in times of the order of 1 μsec.

2) When the force applied to the pressure end of the bar changes instantaneously from zero to a finite value, the pressure deduced from the displacement at the measuring end takes a finite time (after the arrival of the wave) to rise to an approximate constant value. This time depends on Poisson's Ratio and on the radius and length of the bar. When $\nu = 0.29$, with a bar of 0.5 in diameter, 2 ft 3 in long, the time is on the order of 2 μsec; with a bar 1 in diameter, 2 ft 2 in long it is on the order of 3 μsec; and with a bar 1 in diameter, 6 ft long, about 5 μsec.

3) Similar considerations hold when the force at the pressure end is instantaneously reduced from a finite value to zero.

4) It follows that if the pressure to be measured consists of a force which rises instantaneously from zero to a finite value, which is maintained for a time T', and then drops instantaneously to zero, no pretence to accuracy can be made if T' is less than 4 μsec with a bar 0.5 in diameter, 2 ft 3 in long; less than 6 μsec with a bar 1 in diameter, 2 ft 2 in long; and less than 10 μsec with a bar 1 in diameter, 6 ft long.

5) With constant or slowly varying forces, the pressure derived from the displacement at the measuring end fluctuates slightly about its true value. These fluctuations decrease, and the accuracy increases as T' increases. Apart from the initial and final portions of the pulse, an accuracy of about 2% can be theoretically obtained by averaging, if T' is not less than about six times the time taken by the pressure (deduced from the displacement at the measuring end) to reach its final value.

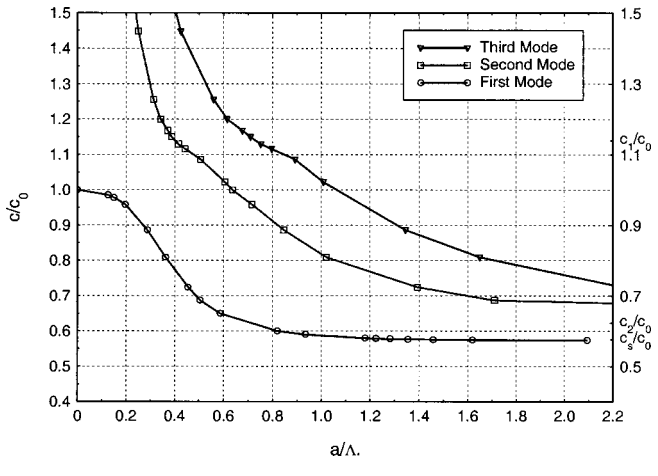

Fig. 6 Phase velocity c of extensional waves of wave-length Λ in cylindrical bars of radius a. $\nu = 0.29$, c_1 = velocity of dilatational waves, c_2 = velocity of distortional waves, c_S = velocity of Raleigh surface waves. In terms of ν, $c_1/c_0 = [1-\nu]/[(1+\nu)\cdot(1-2\nu)]$, $c_2/c_0 = 1/[2(1+\nu)]$. Reconstructed from the data provided in Table 11.1 and Fig. 13, Davies [5], pp 406–407.

H Kolsky [6]: The split-Hopkinson Pressure Bar

In 1949, a year after RM Davies published his critical review of the Hopkinson Pressure Bar method, Kolsky [6] published his famous paper on the measurement of the mechanical properties of several different materials (polythene, rubber, PMMA, copper, and lead) at high rates of loading using a modified Hopkinson Pressure Bar, later known as the ''Kolsky Bar'' or ''Split-Hopkinson Pressure Bar.'' Kolsky used a silver steel pressure bar and increased the length of the time *piece* of Hopkinson Pressure Bar and called it an *extension bar*. He used a thin specimen between the pressure bar and the extension bar and used similar parallel plates and cylindrical condenser units as Davies [5] in measuring the axial and radial displacements under dynamic loading. A good review of literature on the Hopkinson Bar method can be

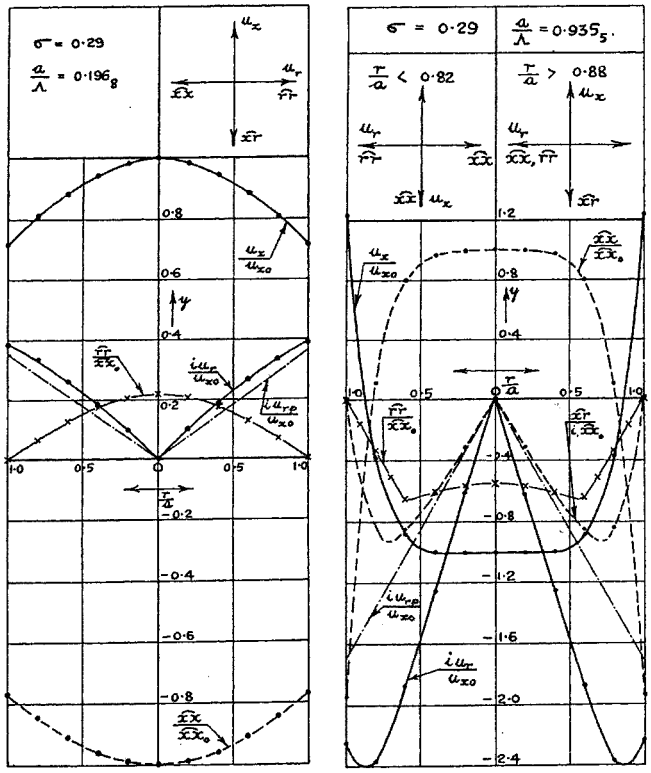

Fig. 7 The variation of the displacements and the stresses over the cross section of a bar of radius a. $x\hat{x}$ = longitudinal stress; $x\hat{r}$ = shearing stress; $r\hat{r}$ = radial stress; u_x = longitudinal displacement; u_r = radial displacement; u_{rp} = radial displacement in distortionless bar. Reproduced from Fig. 19, Davies [5], p 418.

found in Kolsky's paper including B Hopkinson's and RM Davies's work. Kolsky described the modified Hopkinson Bar technique and experimental procedure, derived equations for converting experimental data into the stress and strain of the materials tested, briefly discussed the inertia effect of specimens, and modeled the relaxation behavior of materials tested using a modified Boltzmann [11] model as described by Taylor [12].

General description of Kolsky's apparatus

Figure 8 shows "the general arrangement of the apparatus: similar to that described by Davies except that the bar is in two parts"–the pressure bar (6 ft long, 1 in diameter) and the extension bar (4 in, 6 in, and 8 in long) that can be coupled together with a brass collar. "The specimens, which were in the form of thin disks, were placed between the flat faces of two cylindrical steel bars. The transient pressure was applied by firing a detonator at the end of the bars and the displacement at the free end of the other bar was measured with a parallel plate condenser microphone." In addition, an inertia switch and a cylindrical condenser microphone were also used on the pressure bar. The dynamic data is collected through a cathode-ray oscillograph.

Theory of Kolsky's method

In describing the theory, Kolsky assumed a plane compression pulse propagates without distortion in a linear cylindrical bar. In such a case, the phase velocity is equal to the bar velocity: $c=c_0=\sqrt{E/\rho}$. He also assumed a uniform axial pressure distribution in every cross section. Inherent to this assumption is that the radial stress distribution is linear (which is only true for long wavelengths as compared to the bar diameter). With those assumptions, the pressure in the bar is given by $p=\rho c\dot{u}$, where $\dot{u}$ is the particle velocity.[2] The particle velocity of the free end is twice the velocity in the bar, and thus the pressure in the bar in terms of the free end axial displacement ξ can be expressed as $p=(\rho c/2)\cdot(d\xi/dt)$, as also described by Davies.

Knowing that the axial pressure and displacement are non-uniform in any cross section of the bar (see Davies [5]), Kolsky claimed that "for obtaining stress-strain measurements, any distortion introduced by the main bar does not affect the validity of the results, but only changes the form of the stress cycle to which the specimen is subjected" and "if a sufficiently thin specimen is inserted in the Split-Hopkinson Bar,..., the pressure is effectively the same throughout the specimen during the passage of the compression pulse, and this will be true so long as the thickness of the specimen is small compared with the wavelength of the shortest operative wave in the Fourier spectrum of the pulse."

[2]Kolsky used u instead of $\dot{u}$ to denote particle velocity

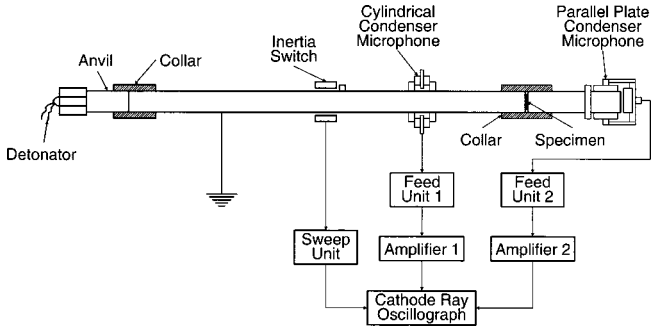

Fig. 8 Schematic of Kolsky's apparatus. Reproduced from Fig. 1, Kolsky [6], p 678.

Derivation of stress-strain relations of the specimen

Both the experimental method and theory described by Kolsky is modified later by researchers and thus is not available in textbooks or articles. It is worth revisiting Kolsky's analysis to make comparison with the theory used mostly by researches today. Following is an exact reproduction of Kolsky's derivation for stress and strain of a thin specimen subjected to dynamic loading.

"Let the pressure of the incident pulse at any time t be p_I, of the transmitted pressure pulse which acts on the specimen p_T, and of the reflected pulse, which is a pulse of tension traveling back along the bar $-p_R$, then

$$p_I=p_R+p_T \tag{9}$$

If we denote the displacement of the face of the main bar in contact with the specimen at time t by ξ_1 we have

$$\xi_1=\frac{1}{\rho c}\int_0^t(p_I+p_R)\cdot dt \tag{10}$$

and if the displacement of the face of the extension bar in contact with the specimen is ξ_2,

$$\xi_2=\frac{1}{\rho c}\int_0^t p_T\cdot dt \tag{11}$$

Now if the thickness of the specimen is z, the fractional strain s is given by $\xi(_1-\xi_2)/z$, hence from (9), (10), and (11) we have

$$s=\frac{2}{\rho cz}\int_0^t(p_I-p_T)\cdot dt \tag{12}$$

Now

$$\frac{2}{\rho c}\int_0^t p_T\cdot dt=\xi_T$$

is the displacement measured by the parallel-plate microphone with the specimen between the bar and the extension, and

$$\frac{2}{\rho c}\int_0^t p_I\cdot dt=\xi_I$$

the displacement produced by the pulse when no specimen is present, the two bars in contact. Thus,

$$s=(\xi_I-\xi_T)/z \tag{13}$$

[3]These Eq. *numbers* are same as in Kolsky [6]

so that if we know the displacement-time relations for ξ_I and ξ_T we can obtain the strain-time curve and, since the gradient of the ξ_T curve gives the stress-time curve, we can derive the stress-strain relation for the material under the conditions of the experiment.''

In Kolsky's derivation of the equations for strain, there are two limitations. First, a negative sign is omitted in the derivation for the displacements ξ, which produces a stress-strain diagram where compressive stresses and strains are presented by positive numbers. Second, p_I is measured using the parallel plate condenser by impacting the main bar and the extension bar together without the specimen, and does not really represent the displacement ξ_1. Kolsky found the displacement measurement of the cylindrical condenser unreliable; however, it was suitable for finding the time reference from the first intercept of the trace on the horizontal axis, ''since the displacement begins rising very slowly, the arrival of the pressure pulse cannot be fixed at all accurately'' from the displacement trace of the parallel plate condenser.

Kolsky discussed the radial inertia effect of the specimen. He made the following suggestions: a) ''this correction was found to be not more than a few percent in most of the experiments''; b) ''and is only important when the rate of straining is changing rapidly''; c) ''the assumption that the expansion is uniform with no frictional effects is not necessarily justified''; d) ''the double differentiation of the strain-time curve may also result in appreciable errors when the correction term is comparable with the actual stress''; e) ''the value of the correction term is proportional to the square of the radius of the specimen and if the method is to be used at higher rates of straining, smaller specimens would have to be employed.''

In describing the calibration of the bar, Kolsky made some additional assumptions, and experimentally proved that his assumptions are valid (Section 4 in Kolsky [6]). He measured the bar velocity from condenser responses and also compared them with the vibration natural frequency method and concluded that that bar velocity obtained from both measurement techniques ''agreed closely.''

Experimental results as described by Kolsky

Kolsky used a specimen diameter ''slightly less than that of the bar, the maximum permissible diameter in each case being determined from preliminary experiments,'' such that the specimens never expand beyond the bar diameter. He used grease between the specimen bar interfaces to reduce friction; however, in the case of rubber specimens, glycol was used. It was found that larger stresses were required to obtain a specific strain in the specimen if no lubricant was being used.

Kolsky mentioned that ''in the limiting case of a very soft specimen the movement of the end face would be very nearly as much as for a free end (0.12 mm). The other face of the specimen in contact with the extension bar would remain almost fixed, and the maximum fractional strain can be given by the ration of 0.12 mm to the initial thickness of the specimen.''

In the case of harder specimens, Kolsky's observation is also very interesting: ''With harder materials both surfaces of the specimen move and the strains are consequently smaller: nevertheless, by using specimens of different thicknesses, the rate of straining and the maximum fractional strain can be varied within certain limit. If the specimens are too thick, the assumption that the pressure on both sides of the specimen are sensibly the same is no longer valid.'' This statement by Kolsky is very important in understanding the stress equilibrium in the specimen (ie, the pressure on both sides of the specimen being sensibly the same). Under dynamic deformation, the general assumption of stress equilibrium is thus questionable.

In Kolsky's method, the strain-time response is calculated from the difference between two displacements (without and with specimens) as described in his theory and the stress-time curve is calculated from the displacement-time curve with the specimen between the bars. Kolsky mentioned that the stress-time curve is corrected for radial inertia effects, and for large deformations, the change in cross-sectional area is taken into consideration. However, his derivation for stress-time does not contain any correction term for the variable area of the specimen (which appeared in literature much later).

Kolsky's work is very important because he tested five different materials (polythene, rubber, PMMA, copper, and lead) and the material behavior of these materials is very different from each other. In the case of polythene (Fig. 9), he reported stress-strain data for four different thickness (0.025 cm, 0.048 cm, 0.086 cm, and 0.768 cm, respectively). The stress-strain plot is represented by a few points where the difference between two consecutive points on the curve represents a time interval of 2 μsec. Data representation of that kind is very useful because the stress-time and strain-time history can be calculated from the stress-strain curve, which is completely ignored in recent literature. Kolsky also

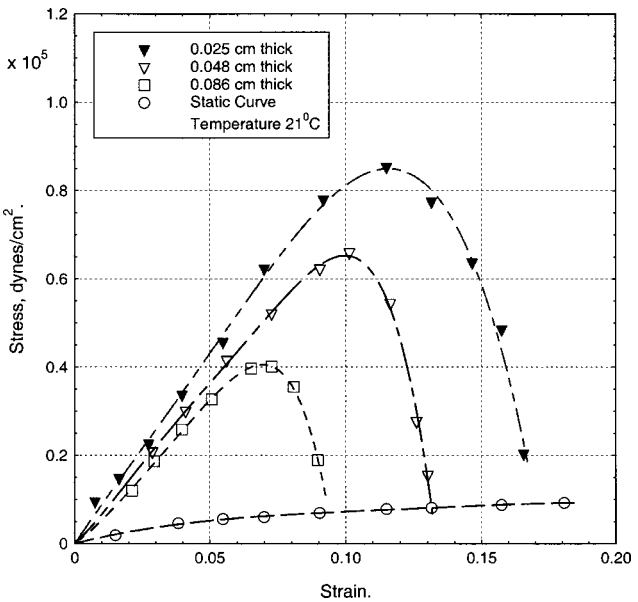

Fig. 9 Dynamic stress-strain behavior of Polythene. Reproduced from Fig. 8, Kolsky [6], p 693.

mentioned that ''to avoid confusion around the origin, the first two or three points on each curve have been omitted.'' This statement reveals that Kolsky did not want to discuss the problems associated with the initial data; however, from Davies's earlier work, it is well known that the initial data is most vulnerable to dispersion effects.

General conclusions from the classic Hopkinson Bar papers

The developments of the Hopkinson Pressure Bar and Split-Hopkinson Pressure Bar techniques are a milestone in dynamic pressure and stress-strain measurement. This apparatus can successfully be used as a dynamic loading device, but the presence of dispersion makes the data representation very difficult, time consuming, and sometimes impossible. As a consequence, when designing experiments, it is necessary to consider specimen geometry, and the specific data analysis of materials because of the different relaxation behaviors of different materials. The controversies involved in the Hopkinson Bar technique are well known and can be found in the literature [13].

Two forms of dispersions are present in a finite diameter pressure bar: 1) The eigen-values of the Pochhammer frequency equation suggests that the phase velocity of propagating harmonic waves in a bar is a function of its wavelength. Generally, high-frequency/low-wavelength harmonic waves propagate slower than low-frequency/long-wavelength waves. The net effect is that any sharp front of a propagating pulse will widen and lose its sharpness. High frequency oscillations (Pochhammer Modes) will be superimposed on the original pulse; 2) The eigen-functions of the Pochhammer solution reveal that the axial displacement is nonplanar and the radial displacements are nonlinear. Therefore, any orthogonal free or partially loaded surface to the bar axis will generate nonplanar deformations of the surface. Any planar assumption of a pressure bar surface will thus not be appropriate in the general case.

Sufficiently thin specimens will ensure that the specimen is under a uniform stress state. Radial inertia effects are important for high rates of loading. In order to reduce inertial effect, smaller specimen diameters can be used. If one fixes the ratio between the specimen to the bar diameter as constant, it might require the use of a smaller diameter bar for high rates of loading. Friction between bar-specimen interfaces is important. The use of a lubricant is recommended in reducing friction effects. The density, bar velocity, elastic modulus, and Poisson's Ratio of the bars should be measured with the highest accuracy because these values are used in the data reduction method.

The calculation of the displacement for soft materials may be straightforward. Displacement measurements on both faces of the specimen are important for hard specimens. Specimen thickness is important for stress equilibrium (which is generally questionable). The correction of the stress-time response for radial inertia is important, and changes in the specimen cross sections need to be taken into account for large deformations. Kolsky's stress-strain data representation, with each point separated by 2 μsec in time, is unique and should be followed in Hopkinson Bar stress-

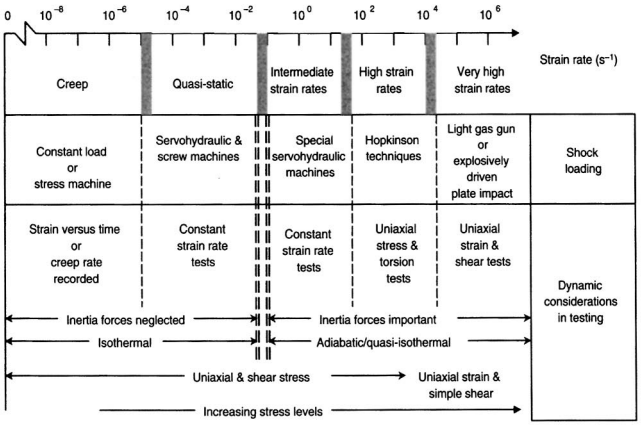

Applicable strain rate, s^{-1}	Testing technique
Compression tests	
<0.1	Conventional load frames
0.1–100	Special servohydraulic frames
0.1–500	Cam plastometer and drop test
200–10^4	Hopkinson (Kolsky) bar in compression
10^3–10^5	Taylor impact test
Tension tests	
<0.1	Conventional load frames
0.1–100	Special servohydraulic frames
100–10^3	Hopkinson (Kolsky) bar in tension
10^4	Expanding ring
>10^5	Flyer plate
Shear and multiaxial tests	
<0.1	Conventional shear tests
0.1–100	Special servohydraulic frames
10–10^3	Torsional impact
100–10^4	Hopkinson (Kolsky) bar in torsion
10^3–10^4	Double-notch shear and punch
10^4–10^7	Pressure-shear plate impact

Fig. 10 Strain rate regimes and corresponding experimental techniques. Reproduced from [17]; Fig. 1 and Table 1, p 427.

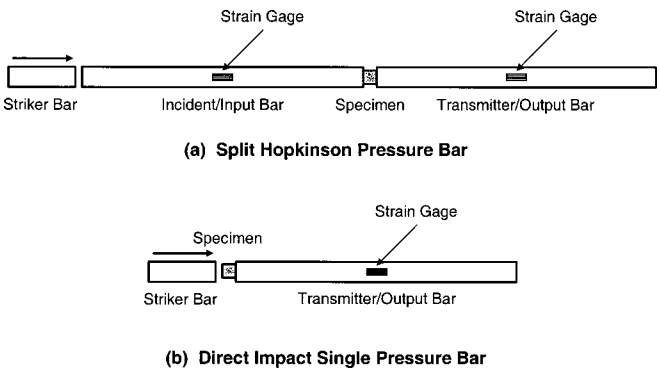

Fig. 11 Typical configurations of the Hopkinson Bar apparatus. Adopted from [18], Fig. 5, p 434.

strain data presentations. The initial portion of the stress-strain curve may contain confusion, if a suitable dispersion correction scheme is not used.

RECENT ADVANCES IN HOPKINSON BAR EXPERIMENTAL TECHNIQUES

Since 1914, research and development on Hopkinson Bar experimental techniques has continued. Researchers have used the classic compression Split-Hopkinson Pressure Bar (SHPB) in testing many engineering materials, ranging from soft to hard; isotropic to anisotropic; homogeneous to non-homogeneous; crystalline, non-crystalline, monolithic, porous; layered, hybrid, and other materials. On the other hand, researchers have developed and/or modified the Hopkinson Bar technique to test materials under tension, torsion, and compression followed by torsion, torsion followed by compression; triaxial loading, and dynamic indentation. In addition, all known quasi-static testing techniques have been subjected to Hopkinson Bar dynamic loadings (eg, shear, flexure, and fracture toughness using notched specimens [14]). Many experimental techniques were designed and built. Special attention was focused on designing the specimen itself to minimize the friction and radial inertia effects, and to ensure a uniform state of stress in the specimen.

The most important part of the Hopkinson Bar technique is the data representation and analysis. Many different schemes and routines are suggested for data reductions, dispersion corrections, and data analysis. The general description of Hopkinson Bar techniques can be found in a number of textbooks [15,16]; however, most of the developments can be found in technical and scientific articles. A recent reference, summarizing the developments of the Hopkinson Bar throughout the twentieth century, is included in the ASM Handbook 2000 Volume 8 [13]. Even with significant advancements in Hopkinson Bar techniques, these methods have not yet been standardized because of the inherent complexity of the data analysis in the presence of dispersion in a finite diameter bar, friction, and the inertia effects on the specimen. In the next section, the state-of-the-art in Split-Hopkinson Pressure Bar techniques, specimen design, and data analysis are presented [13].

State-of-the-art in split-Hopkinson Pressure Bar techniques

Hopkinson Pressure Bar techniques are used to achieve high strain rates in the range of 50 s^{-1} to 10^4 s^{-1} [17], beyond the capability of quasi-static experimental techniques. SHPB experiments are considered uniform uniaxial stress experiments, whereas low velocity plate impact experiments are considered uniaxial strain experiments (Fig. 10). ''Strains exceeding 100% can be achieved with the Hopkinson bar method. The maximum strain rate that can be attained in a Hopkinson bar varies inversely with the length of the specimen'' [17], while the maximum attainable stress in the specimen is limited by the elastic limit of the bar material. If the specimen is in dynamic equilibrium, ''the stress gradient is essentially zero along the sample'' [17]. In order to assure a uniform stress on both sides of the specimen, Kolsky [6] tested circular disc specimens (for polythene) with a thickness between 0.025 cm and 0.268 cm, a bar diameter of 2.54 cm, and specimen diameter ''slightly less than that of the bar.'' Assuming a specimen diameter between 80% and 90% of the bar (the exact specimen diameter was not mentioned in Kolsky's paper), the specimen's thickness to diameter ratio (H_S/D_S) can be found in the range 0.01 to 0.10 (which corresponds to $D_S/H_S = 100$ to 10).

If one assumes that for a thin specimen, the assumption of stress equilibrium is valid,[4] the question arises whether the specimen is under plane stress or plane strain, or under a mixed mode of stress states. If the specimen's diameter to thickness ratio D_S/H_S is less than or equal to unity, the specimen will definitely be under uniaxial stress. If D_S/H_S is greater than one, the mixed mode or uniaxial strain conditions will prevail. Kolsky's experiments with polythene specimens (with $D_S/H_S = 100$ to 10) were, in fact, uniaxial strain experiments.

In its classic form, Hopkinson Pressure Bar techniques have been successfully used to determine the high strain rate flow stress of many elastic-plastic metals, including steel, aluminum, copper, titanium, beryllium, magnesium, zinc, and their alloys [18]. One advantage of materials undergoing large plastic deformation is that the transmitted stress, being ramp-shaped, contains fewer high frequency oscillations (Pochhammer Modes), which guarantees the accuracy of flow stress measurement from the transmitted signal.

The Split-Hopkinson Pressure Bar, as described by Kolsky [6], consists of a one-inch diameter and six-foot long

[4]The validity of stress equilibrium in the specimen is questionable in general.

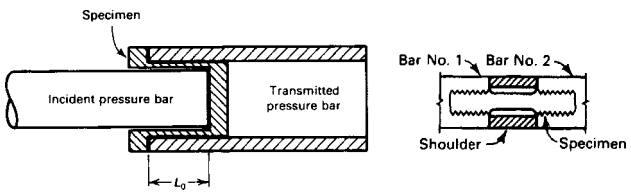

Fig. 12 Techniques developed to use compression SHPB in testing specimens under tension. Reproduced from [18]; Figs. 12 & 14, pp 438–439.

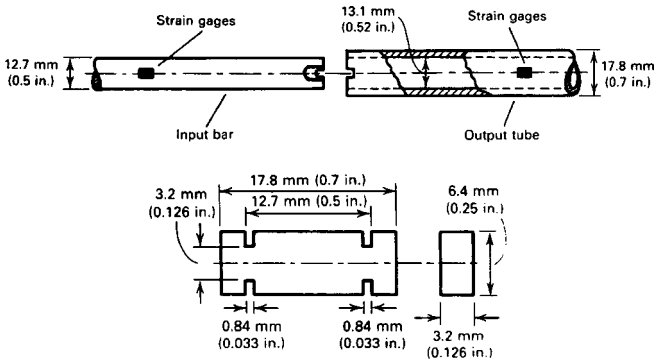

Fig. 13 Techniques developed to use Compression SHPB in testing specimens under double-notch shear. Reproduced from [23]; Figs. 4 and 5, p 450.

pressure bar and a series of *extension bars* of four inches, six inches and eight inches in length. A modern SHPB setup consists of a striker bar, an incident/input bar, and a transmitter/output bar (Fig. 11). Davies and Kolsky used parallel plate and cylindrical condensers to measure the axial and radial displacements of the bars; however, in using the modern SHPB technique, a pair of strain gages are mounted on the surface of the bars at approximately mid-length. The accuracy of strain gage measurements is dependent on the frequency response of the measuring instruments. The strain of the propagating pulse is measured by the strain gage response and recorded through a high-speed data acquisition system or digital storage oscilloscope.

The total time in a classic SHPB experiment is about 1000 μsec or more. Although Kolsky used small extension bars, in modern SHPB techniques, the incident and transmitter bars are equal in length in most cases. A long bar is necessary to resolve the propagating pulses in time without any interference with the reflected pulses,[5] while strain gages are used for recording the data. The strain gage location of the bar downstream from the interfaces, where the pulse is generated, ensures that the uniformity of axial stress is achieved over the entire cross section of the bar, which is an essential condition for 1D stress wave propagation in the bar.

''There are two basic configurations for Hopkinson pressure bar testing: the split-Hopkinson pressure bar and the single pressure bar configuration'' (Fig. 11) [18]. In the Split-Hopkinson Pressure Bar configuration, the specimen is sandwiched between the incident and transmission bars. On the other hand, in the single pressure bar configuration, the specimen is placed on the impact face of the output bar and impacted directly with the striker bar. Although higher strain rates can be achieved with direct impact in the single pressure bar configuration, the displacement of the impact face cannot be measured directly. Therefore, special considerations must be taken into account, eg, high-speed photography [18].

During the past years, modifications of compression SHPB have been made to accommodate dynamic tension, shear, flexure and indentation experiments. Lindholm and Yeakley [19] used a complex top-hat specimen (Fig. 12*a*) in conjunction with a compression SHPB, where the transmitter bar was replaced by a transmitter tube [18]. Another modification of the compression SHPB in conducting tensile tests is described by Nicholas [20]. In this method, a threaded specimen is used between the incident and transmitter bar (Fig. 12*b*), while a thick collar made of the same bar material, and with same outer diameter as the bar is used to protect the specimen from compression loading; and in fact, the tensile reflection from the free end of the transmitter bar loads the specimen in tension.

Shear tests using compression SHPB are also very common. A double-notch shear (DNS) testing [21] and punch loading [22] are described in [23], where an incident bar and a transmitter tube are used in conjunction with double-notch (Fig. 13) and flat plate specimens (Fig. 14*a*). A hat-shaped specimen (Fig. 14*b*) can also be used with traditional SHPB for shear testing [23].

Apart from the Lindholm and Yeakley [19] method and the Nicholas [20] method of tension testing at high rates,

[5]This problem is solved later by separating the ascending and descending waves through one-, two-, and multi-point measurements and will be discussed later.

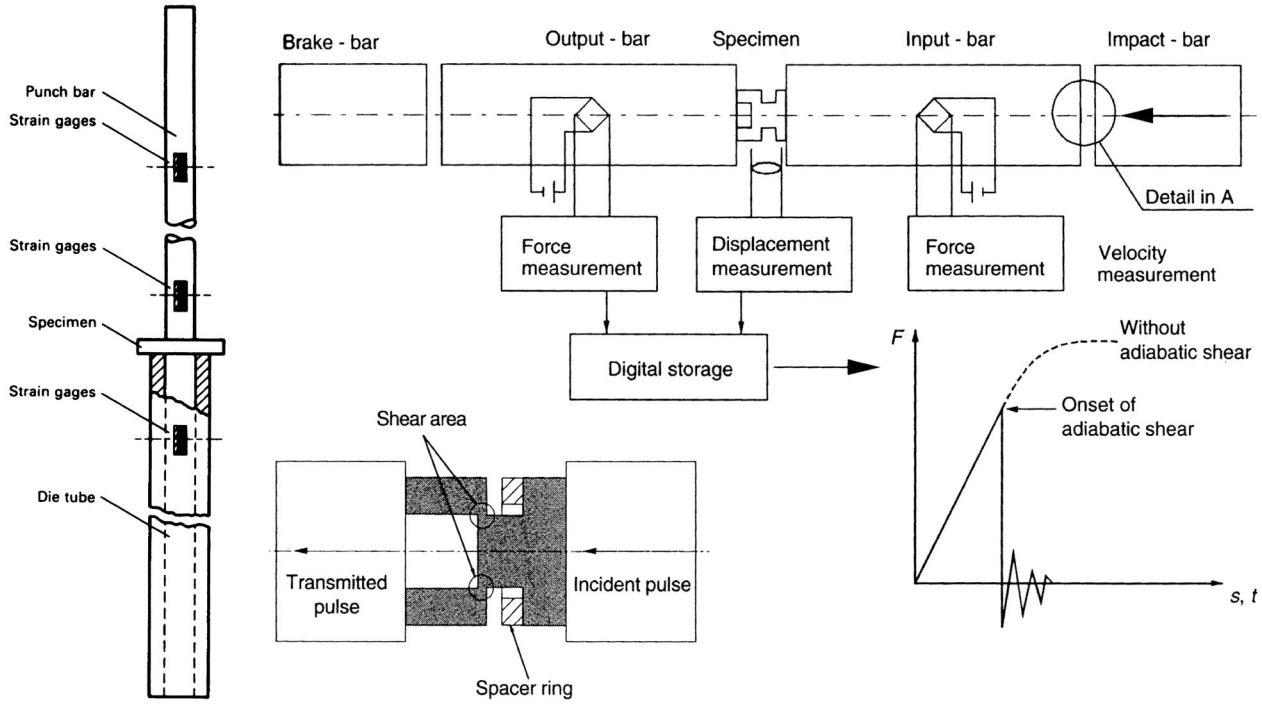

Fig. 14 Additional methods using compression SHPB in testing specimens under shear. Reproduced from [23]; Figs. 6 and 7, p 451.

special tension bars are designed and built [18]. A threaded specimen is fastened between the incident and transmitter bar, while the incident bar is loaded with a tensile pulse generated by impacting a striker tube on the flanged end of the incident bar. The tension SHPB technique is slightly more complex than the compression SHPB technique, because the incident bar should be long and pass through the gas gun (Fig. 15). However, the dispersion effect in the tension SHPB method is similar to those in the compression SHPB technique. The torsion SHPB technique is still more complex than the tension SHPB technique. A very good review on torsion SHPB can be found in [24]. Tubular specimens can be tested under dynamic shear with better confidence, because the first mode of torsion wave propagation in a circular rod is dispersion free [15].

A common problem in compression, tension, and torsion SHPB tests is that the specimen is loaded with reverberating stress pulses more than once. Consequently, the damage observed in the specimen can not be related to the state of stress/loading as obtained from the first reflected and transmitted pulses. In order to resolve this problem, the Recovery Split-Hopkinson Bar was developed as described in [25]. Several methods of momentum trapping are described for both tension and compression recovery experiments. High strain rate testing under a multi-axial loading state has also been developed [26]. In this technique, coaxial bars, tubes, and sleeves are used to load the specimen under multiaxial dynamic states of stress (Fig. 16).

COMPONENTS OF SPLIT-HOPKINSON PRESSURE BAR APPARATUS AND 1D MODEL FOR DATA ANALYSIS

The review of the classic Hopkinson Bar technique was presented in the previous section. However, how the classic SHPB experimental technique and analysis was adapted for the modern SHPB technique is not discussed. An in-depth review of classic SHPB testing is given by Gray III [14], and his derivation and analysis is presented here, in conjunction with that of Davies [5] and Kolsky [6] to study the modern SHPB technique.

Components of a SHPB apparatus

"While there is no universal standard design for SHPB apparatus," most SHPB test apparatus share five common elements:

1) Two long, symmetrical pressure bars with a uniform cross section (usually achieved by precision centerless grinding) of length to diameter ratio (L_B/D_B) in the range 20 to 100 and is usually made from the same materials (eg, maraging steel—E=210 GPa, titanium—E=110 GPa, aluminum—E=90 GPa, magnesium—E=40 GPa or polymeric materials—E<20 GPa). The bar ends are machined orthogonal to the bar axis with high accuracy (no standard tolerance available) to ensure good contact between specimen and bar, and between bar and striker

2) A *bearing and alignment fixture* for correct alignment and to satisfy 1D wave propagation conditions.

3) A compressed gas launcher/gun to propel the striker bars made from same pressure bar material.

4) *Strain gages mounted on both bars to measure the stress-wave propagation in the bars.*

5) *Associated instrumentation and data acquisition system to control, record, and analyze the stress-wave data in the bars.*

Operating principle of a SHPB

In a traditional compression SHPB test, a well designed *right-regular solid*[6] specimen with suitable dimensional tolerance is sandwiched between the incident/input bar (IB) and the transmitter/output bar (TB). The impact of a striker bar (SB) on the impact end of the incident bar produces a compressive stress/strain pulse of geometric length twice that of the striker length [16]. The shape of this pulse in stress-time coordinates is almost rectangular, and the amplitude is proportional to the impact velocity of the striker bar. This pulse propagates toward the incident bar-specimen (IB-S) inter-

[6]Mostly used metallic specimens are right-circular cylinders.

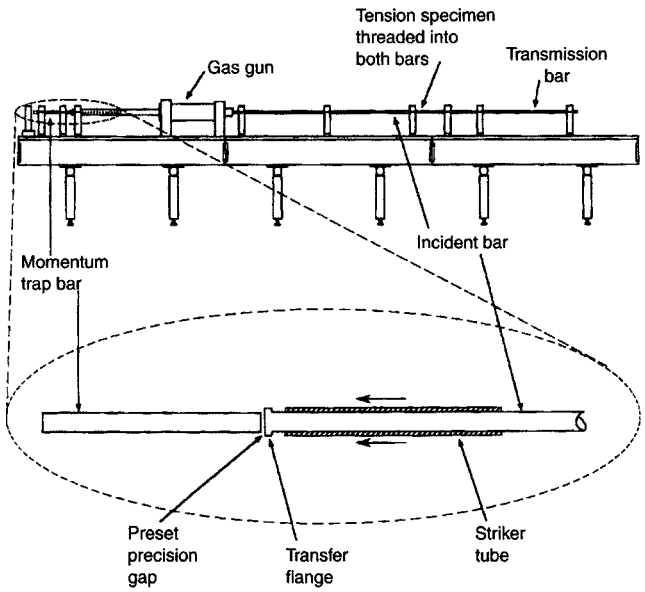

Fig. 15 Recovery tension Hopkinson Bar setup. Reproduced from [25]; Fig. 2, p 478.

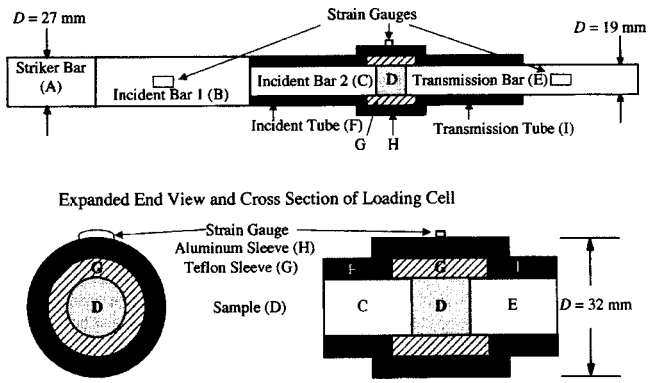

Fig. 16 Triaxial SHPB testing technique. Reproduced from [26]; Fig. 6, p 517.

face, recorded by the strain gage, and is usually denoted by $\varepsilon_I(t)$ and termed as *strain in the incident pulse*. Once the incident pulse reaches the IB-S interface, a complex wave reflection from both the IB-S contact interface and from the IB-S free surface takes place, and the strain gage records the signal, which is termed the *reflected pulse*, $\varepsilon_R(t)$.

In most practical cases, this reflected pulse is tensile in nature and can readily be seen on the strain gage signal having a sign opposite to that of the incident pulse. During the wave reflection from the IB-S interface, a part of the incident pulse propagates through the specimen. A complex reverberation takes place in the specimen between IB-S interfaces and the specimen-transmitted bar (S-TB) interface, until a train of compressive waves are propagated to the transmitter bar. The strain gage mounted on the transmitter bar records the superposition of all the transmissions from the specimen-transmitter bar interface and is termed as the *transmitted pulse* $\varepsilon_T(t)$. During the period of stress wave propagation through the specimen, the specimen undergoes deformation until its dynamic limit is reached.

On a trace of strain gage signals (Fig. 17), the sign of the transmitted pulse appears the same as the incident pulse, but opposite to that of the reflected pulse, if the polarity of the recording devices is set similar for both channels of strain gages on the incident and transmitter bar. By placing the center of the strain gages equidistant from the specimen-bar interfaces, a relative origin in time can be established if both the pressure bars are made from the same materials. Note that the signal presented in Fig. 17 is a conditioned and amplified signal, in which the incident and reflected pulses contain high frequency Pochhammer Modes, while the transmitted pulse contains almost none. It is believed that the viscoplastic deformation of the specimens damps out the high frequency contents of the transmitted signal.

The properties of the bar materials (ρ_B, E_B, c_{0B}, D_B) and the specimen dimensions (H_S, D_S) should be known prior to the data analysis from a SHPB test. For a successful compression test, one has to work with the incident, reflected, and transmitted signals as recorded by the strain gages. The strain gage signals (volts vs time) can be converted to stress/strain in the bar. Finally, an analytical model is necessary to relate the quantity measured—$\varepsilon_I(t)$, $\varepsilon_R(t)$, and $\varepsilon_T(t)$—from the SHPB experiment and the mechanical properties of the materials. It has been identified from Kolsky's [6] derivation that both the average stress and strain of the specimen as a function of time can be calculated from measured quantities. The analytical model that is mostly used in modern SHPB testing can be found in textbooks [15,16]. However, a comprehensive analysis is given by Gray III [14] and is presented below.

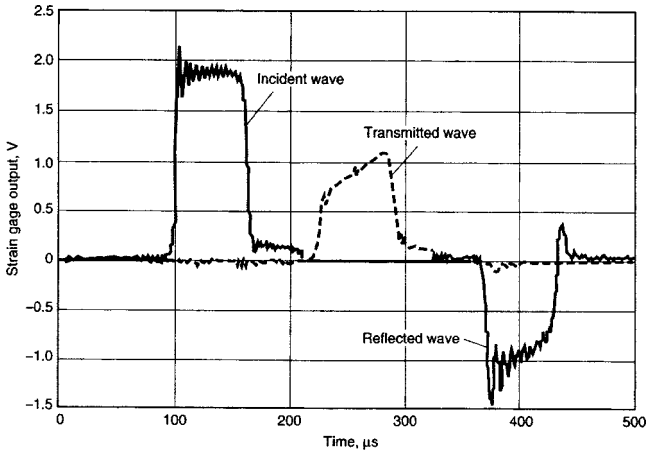

Fig. 17 Strain gage signals obtained from a SHPB test of a 304L stainless steel specimen with a maraging steel bar. Reproduced from [14]; Fig. 3, p 464.

Traditional 1D stress-wave analysis of SHPB

"The determination of the stress-strain behavior of a material being tested in a Hopkinson Bar, whether it is loaded in compression or in a tensile or torsion bar configuration, is based on the same principle of 1D wave propagation" [14]. The 1D stress wave propagation theory in a thin, long rod is based on the fundamental assumptions that the system of bars are linear and dispersion free; which implies that the bars are homogeneous and isotropic, uniform in cross section over the entire length of the bar, the neutral axis of the bar is straight, the material of the bar remains in a linear-elastic state of stress when loaded with propagating stress pulses, and the axial stress distribution is uniform over the entire cross-section of the bar.

Here, the notations used by Gray III [14] are followed: the subscript *1* is used to denote the IB-S interface and subscript *2* is used to represent the S-TB interface (Fig. 18); the displacement at the specimen-bar interface is denoted by u. ε represents the measured strain on the bars, while the subscripts I, R, and T represent *incident*, *reflected*, and *transmitted* pulses, respectively. The arrowheads show the direction of wave propagation. In the case of the bars, the 1D wave equation is given by:

$$\frac{\partial^2 u}{\partial x^2} = \frac{1}{c_{0B}^2}\frac{\partial^2 u}{\partial t^2} \tag{1}$$

Solution of Eq. (1) using D'Alembert's method is given by:

$$u = f(x - c_{0B}t) + g(x + c_{0B}t) = u_I + u_R \tag{2}$$

where f and g are arbitrary functions. The strain is defined by:

$$\varepsilon = \partial u / \partial x \tag{3}$$

Therefore, differentiating Eq. (2) with respect to x, yields:

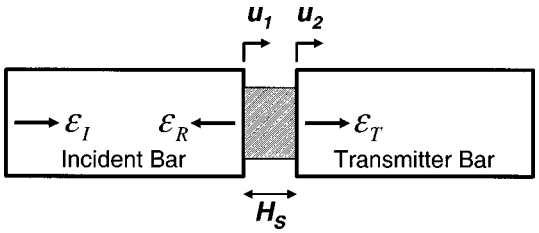

Fig. 18 Traditional/modern 1D Hopkinson Bar analysis. Adopted from [14], Fig. 4, p 465.

$$\varepsilon = f' + g' = \varepsilon_I + \varepsilon_R \tag{4}$$

Differentiating Eq. (2) with respect to t, gives:

$$\dot{u}_1 = c_{0B}(-f' + g') = c_{0B}(-\varepsilon_I + \varepsilon_R) \tag{5}$$

for the incident bar. The time derivative of the displacement in the transmitted bar $u = h(x - c_{0B}t)$ yields:

$$\dot{u}_2 = -c_{0B}\varepsilon_T \tag{6}$$

for the transmitted bar.

''Equations (5) and (6) are true everywhere, including at the ends of the pressure bars'' [14]. Neglecting the stress wave propagation effect in the specimen, the average strain rate of the specimen is:

$$\dot{\varepsilon} = (\dot{u}_1 - \dot{u}_2)/H_S \tag{7}$$

where H_S is the instantaneous length of the specimen, and $\dot{u}_1$ and $\dot{u}_2$ are the particle velocities at the IB-S and S-TB interfaces, respectively. Substituting Eqs. (5) and (6) in Eq. (7) gives:

$$\dot{\varepsilon} = (c_{0B}/H_S) \cdot (-\varepsilon_I + \varepsilon_R + \varepsilon_T) \tag{8}$$

By definition, the forces in the two bars are:

$$F_1 = A_B E_B (\varepsilon_I + \varepsilon_R) \tag{9}$$

and

$$F_2 = A_B E_B \varepsilon_T \tag{10}$$

where A_B is the cross-sectional area, and E_B is Young's Modulus of the pressure bar. It is also assumed that both bars have the same material properties and cross section.

After an initial ''ringing-up'' period, where the exact duration or period depends on the sample sound speed and sample geometry (in particular its length), it is assumed that the specimen is in force equilibrium, and the specimen is deforming uniformly (which implies that friction and inertia effects are negligible). If these assumptions are valid, a simplification can be made equating the forces on each side of the specimen (ie, $F_1 = F_2$). Comparing Eqs. (9) and (10), therefore, means that:

$$\varepsilon_I + \varepsilon_R = \varepsilon_T \tag{11}$$

With the condition of force equilibrium, Eq. (11), the average specimen strain rate, Eq. (8), can be expressed as

$$\dot{\varepsilon} = 2c_{0B}\varepsilon_R / H_S \tag{12}$$

If the constancy of volume is assumed, $A_{S0}H_{S0} = A_S H_S$, where subscript $S0$ represents the original cross-sectional area and thickness of the specimen, strain can be expressed in terms of either the area or thickness of the specimen. For compressible materials, additional specimen diagnostics (eg, high-speed photography) are necessary to calculate the true strain rate and true strain. The average true stress of the specimen is given by

$$\sigma(t) = A_B E_B \varepsilon_T / A_S \tag{13}$$

where A_S is the instantaneous cross-sectional area of the specimen. The calculation of average stress in the specimen using Equations (10) or (13) is known as *1-wave* analysis. If Eq. (9) is used instead, which involves both incident and reflected signals, the analysis is known as *2-wave* analysis, $\sigma(t) = (A_B E_B / A_S) \cdot (\varepsilon_I + \varepsilon_R)$. If both Eqs. (9) and (10) are used to find the algebraic average stress; the analysis is termed as *3-wave* analysis, $\sigma(t) = (A_B E_B / 2A_S) \cdot (\varepsilon_I + \varepsilon_R + \varepsilon_T)$.

The derivation of the 1D analysis of the SHPB experiment described above is extracted from [14], and discusses all the assumptions in sufficient detail. However, the instantaneous thickness (H_S) and cross-sectional area (A_S) of the specimen is not a quantity measured directly from the SHPB test. Therefore, the expressions for average engineering stress and engineering strain of the specimen as a function of time for *1-wave* analysis is given by [16]:

$$\sigma_S(t) = (A_B E_B / A_{S0}) \cdot \varepsilon_t(t)$$

$$\varepsilon_S(t) = (2c_{0B}/H_{S0}) \cdot \int^t \varepsilon_R(t)\,dt \tag{14}$$

Assumptions of a valid SHPB test

Before using the Eqs. (12) and (13) or Eq. (14) in calculating the average stress-strain behavior of the specimen material under high strain rate loading, from the measured quantities of a SHPB test, it is suggested that the validity of the experiment and its assumptions be verified [14]. It is therefore important to prepare the following checklist of assumptions/conditions that need to be satisfied for a valid SHPB test:

1) *Stress wave propagation in the bar is 1D*. The conditions which satisfy this assumption are that the bars are:
   - *a*) homogeneous and isotropic—a condition which can be satisfied by the suitable choice of bar material
   - *b*) uniform in cross-section over the entire length and the neutral axis is straight—centerless grinding of bars can ensure that the cross section is uniform and neutral axis is straight
   - *c*) under a linear-elastic state of stress when loaded with propagating stress pulses—by controlling the impact velocity, it is possible to maintain the stress in the pulse below the elastic limit of the bar material
   - *d*) maintaining uniform axial stress distribution over the entire cross section—following the work of Davies [5], $L_B/D_B > 20$ satisfies this condition
   - *e*) free of dispersion effects—this specific assumption is not valid for a finite diameter bar. Two types of dispersion effects need to be corrected, which will be discussed in the section, Data Processing and Dispersion Correction in SHPB Testing
2) *The incident bar-specimen and specimen-transmitter bar interfaces remains plane at all time*. This condition is described later in the section, A Critical Analysis of Traditional 1D Stress-Wave Theory of SHPB and may be satisfied in general if:

[7] Also in the literature, the strain rate is defined as $\dot{\varepsilon} = (\dot{u}_2 - \dot{u}_1)/H_s$, which differs by a minus sign.

a) the specimen is acoustically soft, ie, low acoustic impedance ($Z=\rho c_0$)
b) the specimen diameter is equal to that of the bar (or a little less than the bar as mentioned by Kolsky [6])
c) a very hard disc is used in the bar-specimen interfaces.

3) *The specimen is in stress equilibrium after an initial "ringing-up" period*. The strain range where this condition is satisfied is usually checked by comparing *1-wave* and *2-wave* analyses, given by Eqs. (9)–(11). In general this assumption is questionable. However, depending on the sound speed of the specimen, a minimum possible thickness may minimize the ''ringing-up'' time, but can not eliminate it.

4) *The specimen is not compressible*. This condition is easily satisfied; however, for soft or nonlinear materials, special analysis techniques should be used. This is discussed in detail in the section, Special Considerations for Soft and Hard Materials

5) *Friction and inertia effects in the specimen are minimum*. This condition can be satisfied by using lubricants in the bar-specimen interfaces, and specially designing the specimen. However, the use of lubricant may also change the acoustic behavior of the interface.

A CRITICAL ANALYSIS OF TRADITIONAL 1D STRESS-WAVE THEORY OF SHPB

In general, the *Traditional 1D Stress-Wave Analysis of SHPB* defines the strain rate of the specimen from the particle velocity of the bar-specimen interfaces, which implies that the bar-specimen interface remains plane under all loading conditions at all times. This condition is true in the case when the specimen diameter is equal to that of the bars, and in the case of acoustically soft specimens, as compared to the bar material (Fig. 19). However, this condition is not true in the case of acoustically hard specimens of smaller diameter than the bar, where the specimen-bar interfaces are nonplanar (Fig. 20). The reflected pulse will thus represent a higher particle velocity of the IB-S interface than the particle velocity of the interface, where the specimen is in contact with the bar, and thus the calculated specimen strain will be higher. The same is true for the S-TB interface.

Figure 20 shows a simple bar-specimen interface model for small diameter hard specimens. However, in reality, deformation behavior of the interface is a superposition of multiple deformation modes. Under the condition of stress equilibrium, it is assumed that the force at the incident bar end and the force at the transmitter bar end near the specimen are equal. And this force equilibrium is achieved *after an initial "ringing-up" period*. This implies that after a couple of stress wave reverberations (3–4, exactly π) [27] in the specimen, the stress equilibrium is achieved.

Comparison between *1-wave* and *2-wave* analyses of a 304 stainless steel specimen shows that the equilibrium is approximately achieved after 2% true strain, and for a high purity lead specimen, equilibrium is never achieved (Fig. 21). These figures also show that the strain rate during the test is not constant, but oscillates over an average value, except in the initial and final stages of loading. This example of stress equilibrium shows that the stress equilibrium in the specimen is dependent on the material behavior (sound velocity and viscosity) and the length of the specimen. Thus, a general statement that the specimen will be in stress equilibrium after 3–4 reverberations is questionable.

From the fact that stress equilibrium is not achieved in the

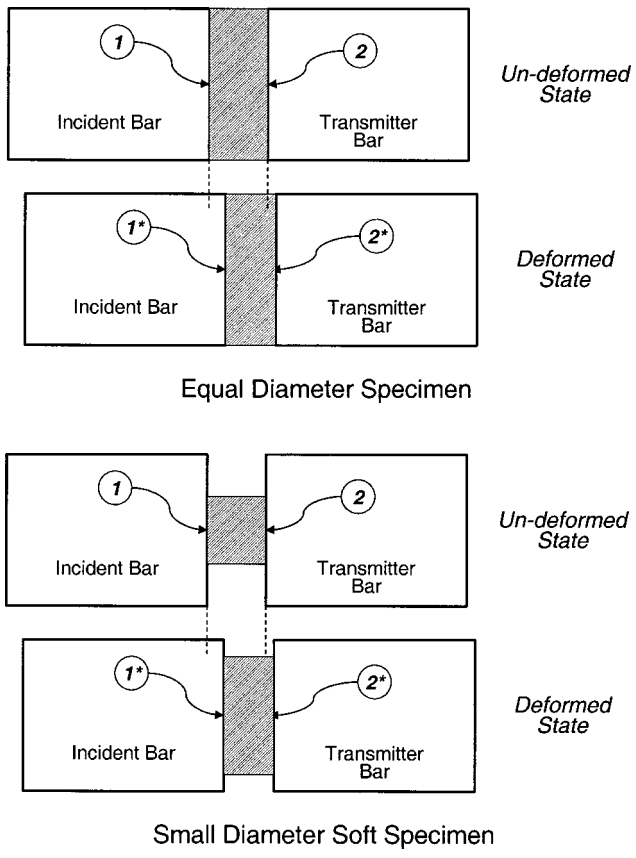

Fig. 19 Conditions for planar bar-specimen interfaces. Numbers 1 and 2 represent IB-S and S-TB interfaces respectively. Symbol * denotes the location of interfaces when the specimen is deformed.

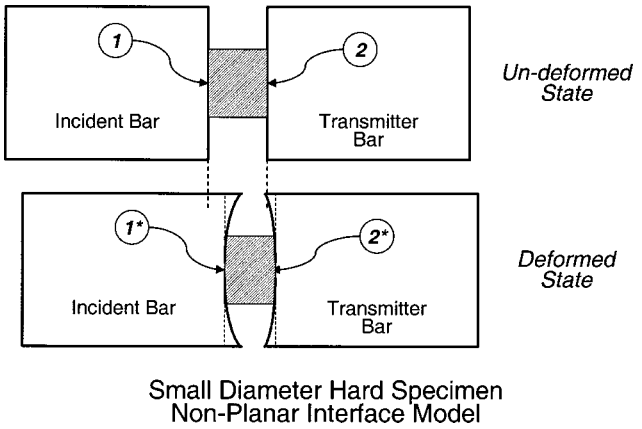

Fig. 20 Deformation of bar-specimen interfaces for small diameter acoustically hard specimens

initial range of small strain, Gray III [14] concluded that ''the finite time to achieve stress-state equilibrium demonstrates that the high-rate elastic modulus of a sample cannot be measured by any Hopkinson bar. Because the stress equilibrium does not occur until well over 1% plastic strain, it is impossible to accurately measure the compressive Young's modulus of materials at high strain rates using the SHPB. The compressive Young's modulus of a material is best measured using ultrasonic techniques.'' Gray III's [14] statement that the dynamic elastic modulus cannot be measured by the Hopkinson Bar method is widely accepted. The question then is what does the stress-strain plot reported in dozens of papers really represent? Can one use the data to extract dynamic material parameters? Due to the controversy in the initial portion of the stress-strain diagram obtained through SHPB testing, many authors simply skip the initial portion of the curve, eg, Kolsky [6], or simply plot stress versus plastic-strain or nonlinear strain [28].

In traditional SHPB analysis, the particle velocity at the specimen-bar interfaces and the stress equilibrium conditions of the specimen, basically defines the boundary conditions of the bar-specimen interfaces, which are derived from logical statements. The conditions of displacement and stress continuity at these interfaces under perfect contact condition, however, should be expressed as:

$$\text{At } x=0: \quad \begin{matrix} u_I(0)+u_R(0)=u_S(0) \\ \sigma_I(0)+\sigma_R(0)=\sigma_S(0) \end{matrix} \tag{15}$$

and

$$\text{At } x=H_S: \quad \begin{matrix} u_S(H)=u_T(H) \\ \sigma_S(H)=\sigma_T(H) \end{matrix} \tag{16}$$

for completeness. In order to satisfy the boundary conditions described in Eqs. (15) and (16); the stress wave propagation in the specimen cannot be neglected, and a higher order formulation considering stress wave propagation in the specimen should be considered. In order to analyze the higher order modes that generate in case of a small diameter hard specimen, the theoretical analysis should be performed in two- and three-dimensions.

GENERAL GUIDELINES FOR SHPB TESTING

Historically, the Hopkinson Bar technique was successfully used in determining the high strain rate flow properties of elastic-plastic metals. Researchers identified that additional care should be taken in testing nonmetallic materials, eg, soft materials [29] and ceramics [30]. However, irrespective of the materials to be tested, each SHPB test method should follow general guidelines. This includes the calibration of the bars; the design of the specimen in terms of expected specimen strain and strain rate; the experiment; and data processing.

Calibration of the Hopkinson Bar apparatus

Calibration of the Hopkinson Bar apparatus is necessary for a new test setup, or if there is a change in the bars, or a change in the strain gages mounted on it. A good review of bar calibration is described in [14]. The strain measured by the strain gages should represent the correct strain/stress states in the bar. A calibration test will thus eliminate any effect of minor misalignment of the gages, or the effect of adhesives used to bond the gages to the bar surface. Two different tests are usually performed: striker bar impact on incident and transmission bars separately (''bars apart''); and striker bar impact on the coupled incident and transmitter bar without any specimen (''bars together''). The former determines the strain correction factors. The latter determines the bar transmission factor or stress correction factor.

The stress in a bar σ_B produced by the impact of a striker bar, according to the 1D wave propagation theory, is given by [16]:

$$\sigma_B=\rho_B c_{0B}\dot{u} \tag{17}$$

where $\dot{u}$ is the particle velocity in the stress pulse. The particle velocity in the bar can be calculated from the momentum balance before and after the impact of the striker bar [16]:

$$\dot{u}=V_{SB}/2 \tag{18}$$

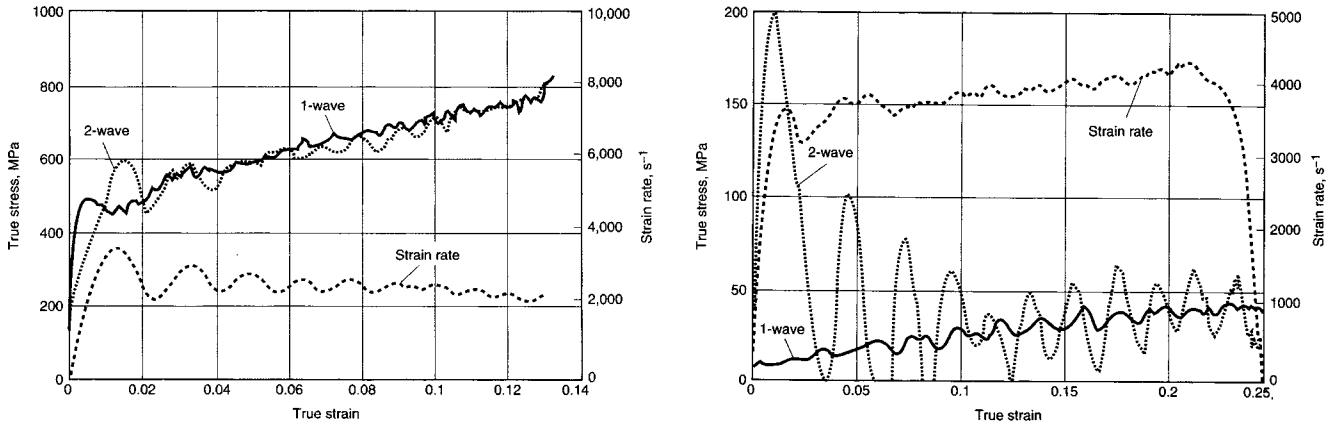

Fig. 21 Test of stress equilibrium through *1-wave* and *2-wave* analysis. Reproduced from [14], Figs. 5 and 6, pp. 467–468.

where V_{SB} is the impact velocity of the striker bar. By correctly measuring the velocity of the striker bars (using laser interruption or shorting pin methods), strain in the pulse can be calculated by:

$$\varepsilon_B^{Calculated} = \sigma_B / E_B = \rho_B c_{0B} V_{SB} / 2E_B = V_{SB} / 2c_{0B} \tag{19}$$

The ratio of the calculated bar strain and the measured bar strain is then termed as the strain correction factor:

$$K_\varepsilon = \varepsilon_B^{Calculated} / \varepsilon_B^{Measured} \tag{20}$$

The strain correction factor K_ε can be determined for incident and transmitter bars separately.

The strain recorded in the incident, reflected, and transmitted pulses can then be corrected as:

$$\varepsilon_i^{Corrected} = K_\varepsilon \cdot \varepsilon_i^{Measured} \tag{21}$$

where i can be substituted for I, R, and T (subscripts used to denote incident, reflected, and transmitted respectively).

In order to calculate the bar transmission factor/stress correction factor, the incident and transmitted bars are coupled together and impacted by the striker bar. The incident pulse is transmitted through the incident-transmitter bar interface, while producing a negligible reflected pulse. This negligible reflected pulse may contain a reflection from the misalignment of the incident-transmitter bar interface and the reflection of higher order modes. The ratio between the amplitude of the incident pulse and the transmitted pulse is called the *bar transmission factor*, or the stress correction factor:

$$K_\sigma = \varepsilon_B^{Incident} / \varepsilon_B^{Transmitted} \tag{22}$$

The calculated average specimen stress can then be corrected as:

$$\sigma_S^{Corrected} = K_\sigma \cdot \sigma_S^{Calculated} \tag{23}$$

where the specimen stress is calculated using Eq. (14).

The density of the bar material can be calculated easily by measuring the weight and volume of the bar. However, an accurate measurement of bar sound velocity c_{0B} is important. Textbook values may not be acceptable [14]. Vibration techniques can be used (as used by Davies [5] and Kolsky [6]). Accurate determination of bar velocity can also be performed through the dispersion correction methodology as described by Lifshitz and Leber [31], or from 1D numerical simulations as described by Zhao and Gary [32,33] and Zhao [34].

The calibration experiments also serve two other specific purposes. If the bar is not aligned, or if the neutral axis of the bar is not straight, or if the impact face of the bar is not orthogonal to the bar axis, the signal recorded by the strain gage will show additional vibration modes in the signal that would otherwise be absent in the case of the ''bars apart'' calibration experiments. If the incident-transmitter bar interface is orthogonal to the bar axes and properly aligned, the transmitted and incident pulse should look alike (within the accuracy of bar dispersion) in the case of the ''bars together'' calibration experiment. If a calibration experiment produces a transmitted pulse much different from the incident pulse, the parallelism of the bar interfaces should be checked; and if necessary, the bar ends be machined with higher accuracy. Once the bars are calibrated, the experiment using specimens can then follow.

Design of specimens for SHPB testing

The design of a specimen is the most critical part of the SHPB experiment. There are no universal rules for specimen design, and often, specimens are designed from exploratory experiments. The design of the specimen should follow the general assumptions made for SHPB technique. The following assumptions are made during a SHPB experiment: a) the specimen deforms uniformly, which implies that there is no friction or no inertia effects; b) the specimen is in stress equilibrium; and c) the specimen is under a uniaxial stress condition. A robust specimen design procedure should satisfy all three of the above conditions. In practice, conditions are sought such that the specimen design is optimum.

Inertia and friction effects

The maximum specimen diameter D_S that can be allowed is equal to the bar diameter D_B. Gray III [14] suggested that the radial and longitudinal inertia and friction effects can be lessened by minimizing the areal mismatch between the bar and specimen ($D_S \approx 0.80 D_B$); and choosing H_S/D_S ratio between 0.50 and 1.0, which is based on the corrections for both longitudinal and radial inertia effects proposed by Davies and Hunter [35]:

$$\sigma_S^C(t) = \sigma_S^M(t) + \rho_S \lfloor (H_S^2/6) - (\nu_S D_S^2/8) \rfloor \cdot (\partial^2 \varepsilon(t)/\partial t^2) \tag{24}$$

where subscript S stands for *specimen*, and superscripts C and M stand for *corrected* and *measured*, respectively. The second term of Eq. (24) is a correction term to be added with the measured average stress of the specimen. The correction term will be zero, if either the strain rate is constant or the bracketed term is zero. The later condition provides the optimum ratio of the specimen for inertia effect and is expressed as:

$$H_S/D_S = \sqrt{3\nu_S/4} \tag{25}$$

For a Poisson's Ratio of 0.333, the optimum H_S/D_S is 0.50. According to ASTM E 9, Compression Testing of Metallic Materials at Room Temperature, to minimize the friction effects, the H_S/D_S ratio should be in the range 1.50–2.00. Thus the conditions for minimum friction and inertia effects can not be satisfied simultaneously and Gray III's [14] suggestion of $0.50 < H_S/D_S < 1.0$ can be taken as a compromise between these two effects. While using specimen $H_S/D_S < 1.5$, researchers used lubricant to reduce friction, eg, oil-based molybdenum disulfide for room temperature, and fine boron nitride powder for high temperature test conditions. Efforts have also been made to quantify the friction using annular specimens [36].

If a constant strain rate condition is used, then one can effectively use thinner specimens ($H_S/D_S < 0.50$), and thus minimize the stress nonequilibrium in the specimen. Usually, constant strain rate conditions can be achieved through

shaped incident pulses, however, the attainable strain rates in these cases are limited by the stress rate of the incident pulse [30], and is described next.

Stress equilibrium, uniaxial stress and pulse shaping

The optimum thickness of the specimen depends on the rise time t required to achieve a uniaxial stress state in the specimen. The rise time is estimated as the time required for π reverberations in the specimen [37]. For a plastically deforming solid that obeys the Taylor-von Karman theory, the rise time is given by:

$$t^2 \geqslant (\pi^2 \rho_S H_S^2)/(\partial\sigma/\partial\varepsilon) \tag{26}$$

where ρ_S and H_S are the density and thickness of the specimen, respectively, and $\partial\sigma/\partial\varepsilon$ is the Stage 2 work-hardening rate of the true stress-strain diagram of the material to be tested. By decreasing the specimen thickness, it is thus possible to reduce the rise time; however, the specimen H_S/D_S requirement for minimizing friction and inertia effects require that the specimen diameter also be reduced. Therefore, one needs to use a smaller diameter bar as well (to satisfy the conditions, $D_S \approx 0.80 D_B$ and $0.50 < H_S/D_S < 1.0$). Kolsky's [6] experiment, with $0.01 < H_S/D_S < 0.10$, thus does not represent a uniaxial stress case.

One way of reducing the rise time in the specimen is the use of a shaped pulse. The rise time of a near rectangular pulse, generated by the direct impact of the striker bar, is generally smaller than the rise time of the specimen. If a thin elastic-plastic metal disk (tip material, [14]) is used between the incident and striker bar, a ramp shaped incident pulse with almost constant stress rate can be achieved.

The use of such a ramp shaped incident pulse should theoretically generate a constant reflected pulse, which according to 1D SHPB theory represents a constant strain rate of the specimen. A constant strain rate test condition is an essential condition of a valid material characterization test. According to Eq. (24), such a test can be performed on any specimen H_S/D_S ratio, satisfying the minimum friction condition.

The pulse-shaping technique was first introduced in testing ceramic specimens [30], when researchers observed that ceramic specimens fracture prematurely, before the stress equilibrium is achieved. Use of a shaped pulse solved this problem. A ramp-shaped pulse also contains almost no high frequency oscillations (Pochhammer Modes), and thus the dispersion effect is minimal. Although the pulse shaping generally reduces the achievable strain rate in the specimen, in order to satisfy the constant strain rate condition in the specimen, every SHPB test should use a shaped pulse irrespective of the kind of specimen materials (soft, hard, nonhomogeneous, brittle, nonlinear, etc). The strain rate and total strain in the specimen can then be varied by a suitable choice of a *tip material or pulse-shaper* geometry, the striker bar length, and the impact velocity of the striker bar.

Other considerations

It is important that the specimen made from a particular material contains multiple units of its repeating structure to represent the bulk properties. This condition is important in the case of large grain polycrystalline materials, particle- and fiber-reinforced composites, and cellular materials. Coarse material structures often require a larger bar diameter (a 75 ~100-mm diameter bar is required to test concrete). Brittle materials, like ceramics, require a special specimen design to ensure uniform stress before failure. Tracy [38] used *dog-bone* specimens to ensure uniform stress in ceramic specimens. Couque *et al* [39] used tapered specimens with chamfered rings to suppress axial splitting in case of composite specimens. The use of nonuniform sections along the specimen length makes data reduction more complex. The tolerance in specimen geometry is important to ensure uniform deformation. Gray III [14] mentioned the loading faces of the specimen must be parallel within a tolerance of 0.01 mm (0.001 in) or better.

Special considerations for soft and hard materials

It is well accepted in the Hopkinson Bar research community [13] that SHPB experimental methods and 1D data analysis is generally valid for elastic-plastic metals that satisfy the conditions mentioned in the section, Assumptions of a Valid SHPB Test. However, additional difficulties arise in the case of soft and hard materials, which include all kinds of engineering materials other than elastic-plastic metals. The ASM Handbook [13] devotes two separate sections on the SHPB testing of soft materials [29] and ceramics [30]. One must read these sections before testing similar materials.

SHPB testing of soft materials

Soft materials include a wide variety of polymeric materials, foams of metals and polymers, and granular materials. This class of materials is characterized by their very low acoustic impedances, and under SHPB testing conditions, generate very weak/poor transmitted pulses if the traditional steel bar with high gain is used. Researchers used low impedance bars (titanium, aluminum, and magnesium bars [40,41]) where good transmission signals can be obtained. Others used polymeric bars [42–44] (PMMA, PC) in testing soft materials. The use of a polymeric bar requires additional analyses of the visco-elastic bar behavior, adding more complexity compared with low impedance metallic bars. In addition to the low impedance solid metallic and polymeric bars, Chen *et al* [45] used a hollow aluminum transmission bar to obtain better signal to noise ratio over solid bars. The main issue in testing soft materials is to obtain a good transmitted pulse, which can be achieved by the use of low impedance bars. However, all the assumptions of stress equilibrium, uniform and uniaxial stress, inertia and friction effects, and dispersion conditions need to be satisfied for a valid SHPB experiment.

The low wave speed in soft materials makes the transit time in the specimen much longer than metallic materials. Thus, a thin specimen is necessary to satisfy the stress equilibrium condition. In fact, strong dependence of H_S/D_S ratio on the stress-strain behavior of soft materials is found [29]. Chen *et al* [45] observed substantial wave attenuation in thick (0.25 inch) RTV630 rubber samples as compared with thin (0.06 inch) samples, suggesting that depending on test temperature and specimen material, a H_S/D_S ratio of 0.25–0.50 can be used to minimize attenuation.

''Due to the soft, viscoelastic nature of some polymers and polymeric composites at ambient temperatures, a special procedure has been adopted at Los Alamos National Laboratory to machine SHPB specimens with parallel loading surfaces within a tolerance of 0.03 mm (0.001 in.)'' [29]. The rough cut specimen is cooled down well below its glass transition temperature using liquid nitrogen, and is then machined in its hardened state; and slowly warmed up back to room temperature.

Gray III [14] suggested that a combined finite element analysis of a SHPB experiment can be useful in reducing the experimental data with confidence, designing the SHPB experiment, and using nonstandard Hopkinson Bar experimental techniques. SHPB testing of porous and granular materials requires additional sample diagnostic tools, such as high-speed photography and coupled Lagrangian analysis [14].

SHPB testing of hard materials

The article, *Split-Hopkinson Pressure Bar Testing of Ceramics*, by Subhash and Ravichandran [30] in the ASM Handbook [13], clearly states the general assumptions of the Hopkinson Bar experiment as described in earlier sections. In fact, many questions raised about the validity of the generalized Hopkinson Bar technique are first asked when researchers have tried to test ceramics, which are very hard and almost linear elastic materials, with a few exceptions for materials with stress-induced transformation and microcracking (eg, magnesia partially stabilized zirconia—MgO-PSZ).

Most ceramics possess a high stress wave velocity, ensuring a very small transit time. It has been identified that the loading of ceramic specimens with a rectangular pulse will fracture the ceramic specimen, even before the specimen reaches stress equilibrium. A way of slowly loading the specimen is sought to avoid this problem. Also, notice that in order to study the fracture behavior of ceramic specimens, it should only be loaded with one single pulse, and all the successive reverberating pulses should somehow be prevented from loading the specimen.

The indentation of ceramic specimens in the loading end of the bars violates the assumption that the loading surface remains plane at all times (as discussed in the section, A Critical Analysis of Traditional 1D Stress-Wave Theory of SHPB). Because most ceramics fracture at about 1% strain, a way of measuring small strains needs to be devised (as previously discussed, the nonequilibrium in the specimen during the initial loading phase and dispersion effects make the measurement of small strains unreliable). Apart from these challenges, all other conditions/assumptions of classic SHPB testing equally apply in the case of testing hard materials. Other than ceramics, any other material which shows linear-elastic behavior and brittle failure (eg, unidirectional composites in the fiber direction), all the conditions described for ceramics equally apply.

The slow loading of ceramic specimens by a ramp pulse is performed by pulse shaping [46]. ''A ramp pulse can be produced by placing a thin ductile (eg, copper, aluminum) metallic disk of 0.5 to 1 mm (0.02~0.04 in) thick and 2 to 3 mm (0.08~0.12 in) diameter on the impact end of the incident bar.'' The direct impact of the striker bar on the pulse shaper/tip material will plastically deform the pulse shaper and generate a ramp-shaped pulse (Fig. 22). The rise and fall of the ramp pulse can be controlled by a suitable choice of tip material, and the length and velocity of the striker bar. If one needs to use a shaped pulse, it is necessary to create a design chart of pulse shaper parameters, including the material properties of a pulse shaper, geometric dimensions, length, and impact velocity of the striker bar for different bar diameters and materials.

Loading the ceramic specimens with a controlled single pulse up to a certain strain level is generally performed by stress-reversal momentum trapping techniques (eg, Fig. 14 for tension SHPB) developed by Nemat-Nasser *et al* [25]. Various momentum trapping techniques have been developed for both compression and tension recovery Hopkinson experiments. In its simple form, a flanged IB with a concen-

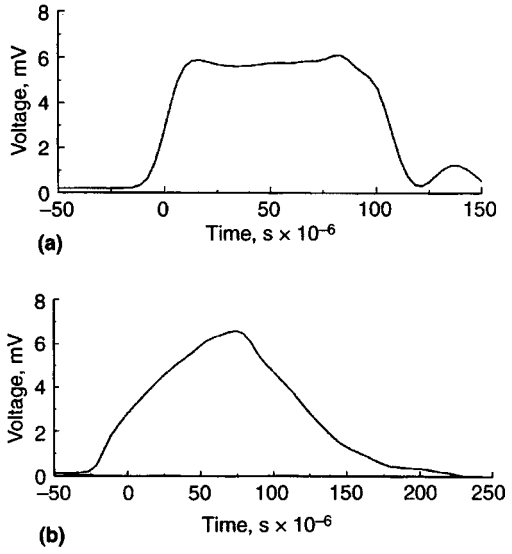

Fig. 22 Comparison of a) rectangular-shaped pulse with b) ramp-shaped pulse obtained from the same length striker bar. Reproduced from [30], Fig. 8, p 501.

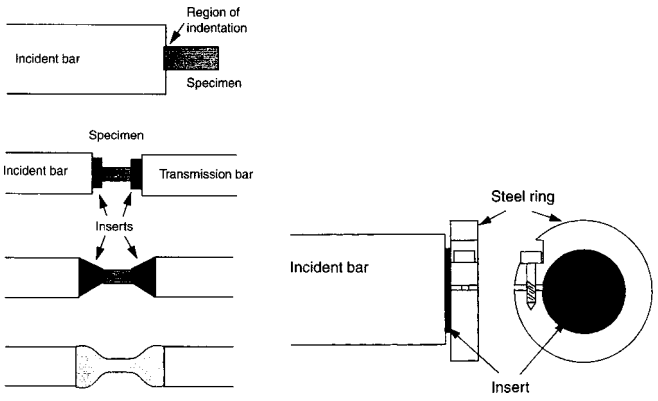

Fig. 23 Ceramic specimen design a) problem of indentation, impedance matched WC inserts, conical inserts, and dog-bone specimen b) steel ring lateral confinement for WC inserts. Reproduced from [30], Figs. 3 & 4, p 499.

tric cylindrical tube is used as the stress-reversal momentum trapping device. In compression SHPB, a predetermined gap is set between the flange and the tube (other end of which is supported to a rigid body). Upon the impact of the SB, a compression stress pulse propagates through the IB, and depending on the gap between the flange and the tube, a compressive wave also propagates through the tube and reflects back as compressive from the rigid support. This reflected compressive stress pulse applies a compressive force on the flanged end, which ultimately generates a tension pulse in the IB. By suitable choice of the length of the tube, the gap, and the length of the striker bar, a compressive pulse followed by tension pulse can be generated; which guarantees the loading of the specimen by a single compressive pulse of specific duration. Like pulse shaping, these momentum trapping and recovery experiments can be equally applied to any materials of interest.

The specimen design in testing ceramics is also very important. The tolerance of loading faces is more important in the case of ceramics because of their low strain to fracture. Any surface flaws will cause premature failure modes such as chipping. ''It is extremely important to grind the end surfaces to a high degree of flatness (at least 0.01 mm, or 0.004 in) and parallelism (within 0.001 mm, or 0.00004 in) to avoid premature failure of the specimens'' [30]. For the same reason, the preferred length of ceramic specimens is to be longer than the metallic specimens to allow for a larger displacement of the bar end before specimens fracture. The recommended H_S/D_S ratio for metals is between 0.5 and 1.0, the H_S/D_S ratio for ceramics between 1.0 and 2.0 is recommended [30].

One of the problems of using a metallic bar in testing ceramics is the indentation created by the specimen in the bar. Therefore, the assumption that the bar ends remain flat during loading is violated. This problem can be solved using thin impedance-matched tungsten-carbide (WC) inserts between bar-specimen interfaces (Fig. 23*a*). In order to prevent the failure of WC inserts, a special steel confinement has been proposed (Fig. 23*b*). Conical insert geometry [47] and dog-bone shaped specimens [48,49] are also considered in SHPB testing of ceramics.

Although a ramp-shape incident pulse contains a minimum number of high frequency oscillations (Pochhammer Modes), measurement of small strains from the reflected pulse (1D SHPB analysis) is not reliable. In addition, the use of WC inserts, conical inserts, and dog-bone specimens make the interpretation of strain obtained from the reflected pulse difficult. It is suggested that a pair of strain gages (axial and transverse) be mounted to monitor the strain of the specimen [30]. However, the size effect of strain gages on the measured strain needs to be understood.

The stress equilibrium in the specimen is generally checked by *1-wave* and *2-wave* analyses, where it is believed that the *2-wave* stress-strain curve oscillates equally below and under the curve obtained from *1-wave* analysis [14,29]. However, this is only a qualitative check. Ravichandran and Subhash [50] showed that the dimensionless stress difference between the ends of the specimen (stress nonequilibrium factor) become less than 10% of the mean specimen stress if the time is greater than four times the transit time in the specimen (Fig. 24). Finite element analysis can also be performed to compute these relationships [51].

However, Fig. 24 shows that in any case the specimen is not in complete stress equilibrium and Eq. (11) does not hold true, rather the following relation exists:

$$(\varepsilon_I+\varepsilon_R-\varepsilon_T)=\Phi(\varepsilon_I) \tag{27}$$

In the light of the discussion about stress equilibrium in a specimen of any kind in SHPB testing, it can generally be concluded that the specimen is never in stress equilibrium for the traditional specimen thickness in the diameter range $0.25<H_S/D_S<2.0$ (from soft to hard) [52]. Although Kolsky's [6] specimens, $0.01<H_S/D_S<0.10$, do not satisfy the criteria for optimum inertia and friction effects, thin specimens might have better stress equilibrium. The issue of stress nonequilibrium in the specimen may be addressed by plotting stress versus strain rate, instead of stress versus strain.

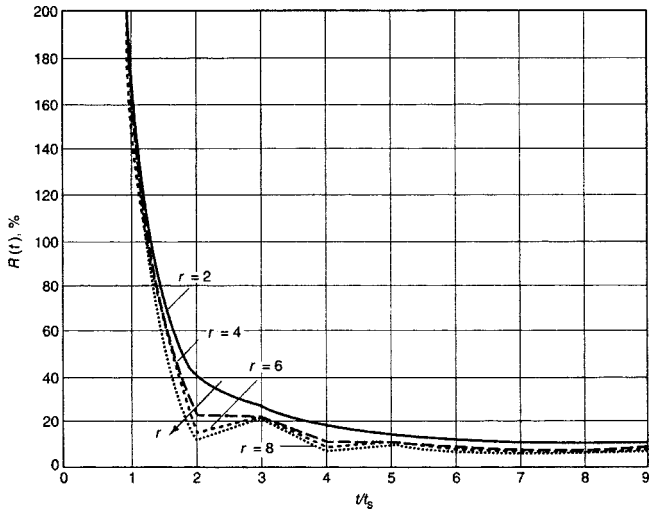

Fig. 24 Normalized stress difference (stress non-equilibrium factor) between ceramic specimen ends as a function of number of wave reflections. Reproduced from [30], Fig. 2, p 498.

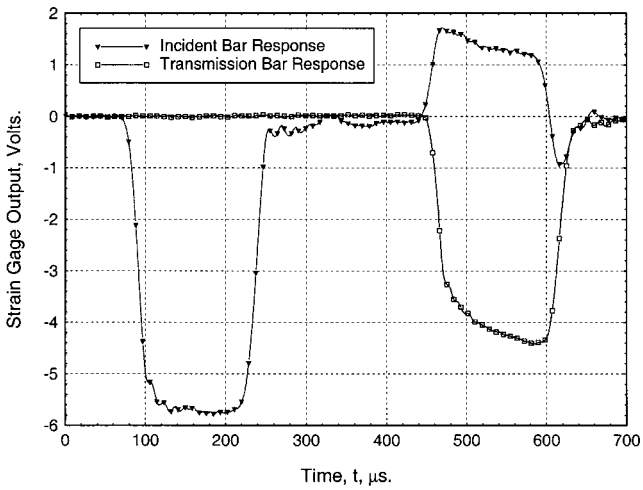

Fig. 25 Typical strain gage records of SHPB experiment

Because the specimen is not in equilibrium, a time-averaging of the non-equilibrium stress-time and strain-rate-time data may have engineering values if the time-averaging window is taken larger than one characteristic time, $\tau_S = H_S/c_S$, of the specimen.

DATA PROCESSING AND DISPERSION CORRECTION IN SHPB TESTING

Processing of the Hopkinson Bar signal into engineering data is not straightforward. It is well known that the dispersion effects need to be corrected for better data representation [31,53,54]. This requires the accurate determination of the bar properties (E_B, ρ_B, ν_B, c_{0B}) and starting points, or zeros, of individual signals/pulses, use of Fourier integrals to convert the time domain Hopkinson Bar data into discrete frequency domain data, use of the Pochhammer [6] frequency equation in determining phase velocities of discrete Fourier frequencies, computation of new phase angles from phase velocities of discrete frequencies, and an inverse Fourier transformation back to the time domain. The following sections describe each operation in further detail.

Data processing

The dimensions of the specimen are known before a Hopkinson Bar experiment is performed. After the experiment is complete, the user has a record of the strain gage signals and the recovered specimen. The strain gage signals can then be converted into strain in the bars, and thus the incident $\varepsilon_I(t)$, reflected $\varepsilon_R(t)$, and transmitted $\varepsilon_T(t)$ strains are obtained. Before using Eq. (14) for *1-wave* analysis, or other operations for *2-* and *3-wave* analyses, one should identify the starting point of these strain pulses and correct the data from dispersion effects.

Usually, strain gages are mounted on the bars equidistant from the specimen-bar interfaces. The recorded strain gage signals of reflected and transmitted pulses thus represent the state of the IB-S and S-TB interfaces at the same time (Fig. 25). If the thickness of the specimen is very small compared to its diameter ($H_S/D_S \sim 0.0$), the start of reflected and transmitted pulses should ideally correspond to the same time. If the H_S/D_S is on the order of 1.0, and/or the impedance of the specimen is less than that of the bars, a significant time delay will be noticed between the starting point of the reflected and transmitted pulses. If the location of the strain gages are not equidistant from the bar-specimen interfaces (intentional as in Fig. 14, or error in placement of gages), identifying the starting point of a pulse in time will be a challenge.

In the case of *1-wave*, *2-wave*, or *3-wave* analysis, algebraic operations on the incident, reflected, and transmitted pulses are performed, which requires an accurate identification of the starting point in time for these pulses; and to transform them to a common zero on a time axis. The dispersion in the propagating pulse also introduces an initial portion of the pulse with a slow rise, which makes the identification of a *zero* point difficult. It is preferable that the identification of the *zero* points be performed during dispersion correction [31], or from 1D simulation [32–34].

Dispersion correction

The idea of dispersion correction of the Hopkinson Bar response is due to Pochhammer [6] and Chree [7]. Pochhammer solved the stress wave propagation in an infinite rod of finite diameter in 3D. He obtained the following frequency equation for a propagating harmonic wave.[8]

$$\frac{4\pi^2}{\Lambda^2}\left(\frac{\rho c^2}{\mu}-2\right)J_1(ga)\cdot\left[2\mu\frac{\partial^2 J_0(ga)}{\partial a^2}-\frac{4\pi^2\lambda\rho c^2}{\Lambda^2(\lambda+2\mu)}J_0(ga)\right]+\frac{16\pi^2\mu}{\Lambda^2}\frac{\partial J_0(ga)}{\partial a}\frac{\partial J_1(ha)}{\partial a}=0 \tag{28}$$

[8] In this section, symbols E, ρ, c_0, and ν are used without subscript B to represent the properties of the bars.

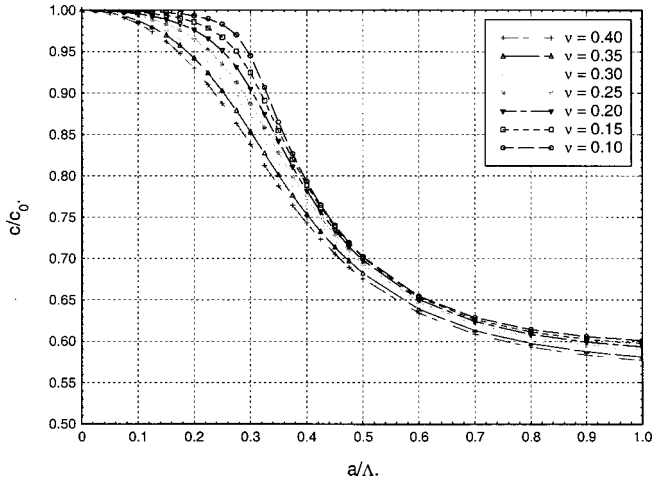

Fig. 26 Dimensionless phase velocity c/c_0 as a function of a/Λ. Reproduced from [9], Table I, p 589.

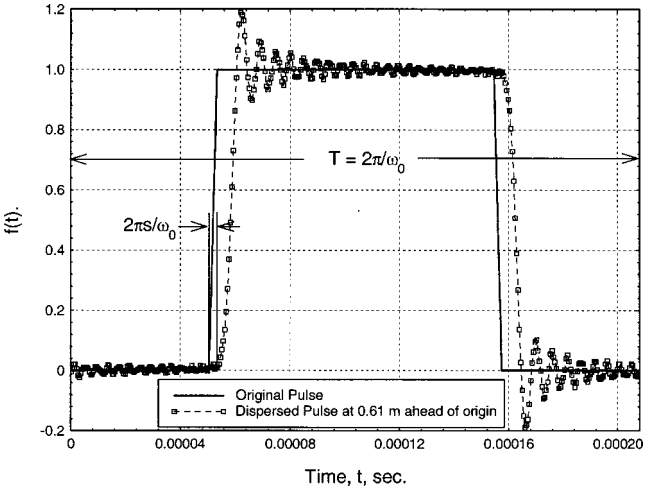

Fig. 27 Dispersion of a trapezoidal pulse after traveling 0.61 m in a 4.6 mm diameter bar with $\omega_0 = 3.021\times10^4$ s^{-1}, $c_0 = 4830$ m/s, and $\nu = 0.29$

where

$$g=\frac{\Lambda}{2\pi}\left[\frac{\rho c^2}{\lambda+2\mu}-1\right]^{0.5},$$

$$h=\frac{\Lambda}{2\pi}\left[\frac{\rho c^2}{\lambda}-1\right]^{0.5},\quad \frac{\partial()}{\partial a}=\frac{\partial()}{\partial r}\Big]_{r=a},$$

J_0 and J_1 are the Bessel function of the first kind of order zero and one, respectively, a is the radius of the bar, λ and μ are Lame's constants, ρ is the density of the bar, and c is the velocity of wave propagation of harmonic excitation of wavelength Λ. The solution for the first mode of this frequency equation was first published by Bancroft [10] and later by Davies [5] (first three modes for $\nu=0.29$, Fig. 6) in the form of tables. Bancroft's solution is reproduced in Fig. 26, where the dimensionless wave velocity c/c_0 is plotted as a function of a/Λ for different values of Poisson's Ratio ranging from 0.10 to 0.40. This solution tells us that the wave propagation in a cylindrical rod is dispersive in nature meaning that $c=f(\Lambda)$.

If a propagating pulse contains many frequencies, the higher frequency harmonics having short wavelengths will propagate slower than the low frequency-long wavelength waves. The net effect is that a sharp pulse will widen its shape and a lot of oscillations will appear as it propagates along the bar (Fig. 27). Figure 26 also shows that the Poisson's Ratio of the bar also has a significant effect in wave dispersion, thus an accurate determination of Poisson's Ratio of the bar material is important. This can be performed by placing a 0/90 strain gage on the bar, or testing tensile coupons made from the same bar material.

Yew and Chen [55] showed that the dispersion characteristics of longitudinal waves in their aluminum bars belonged to the first mode of vibration, which is later confirmed by Follansbee and Frantz [53]. Follansbee and Frantz [53] revisited Davies's [5] method to show that if a trapezoidal pulse is propagating in a bar, its dispersive characteristics can be predicted using Fourier transform. Consider a trapezoidal pulse (Fig. 27),

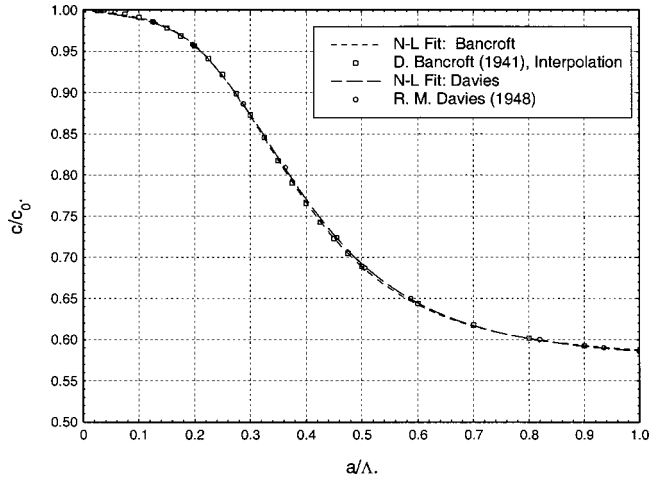

Fig. 28 Comparison between Bancroft's [10] and Davies's [5] data, $\nu=0.29$

Table 1. Nonlinear fitting parameters of Bancroft's and Davies's dispersion data

Fitting Parameters	$\nu=0.29$	
	Bancroft [10]	Davies [5]
A	0.57594	0.57283
B	0.42555	0.42725
C	21.326	16.048
D	19.224	20.339
E	−7.3258	−7.3040
F	2.4713	2.4274

$$F(t)=|F(t)|_0\cdot f(t) \tag{29}$$

with period $T=2\pi/\omega_0$ and rise $2\pi s/\omega_0$, which can be expressed as an exact Fourier series.

$$f(t)=\frac{F(t)}{|F(t)|_0}=\frac{1}{2}-\frac{2}{\pi^2 s}\sum_{k=1,3,\ldots}^{\infty}\frac{1}{k^2}\times(-1)^{(k-1)/2}\sin(\pi k s)\cos(k\omega_0 t) \tag{30}$$

If the discrete frequencies travel at different phase velocities, then at a distance x, away from the origin, Eq. (29) can be expressed as:

$$f(t)=\frac{F(t)}{|F(t)|_0}=\frac{1}{2}-\frac{2}{\pi^2 s}\sum_{k=1,3,\ldots}^{\infty}\frac{1}{k^2}(-1)^{(k-1)/2}\times\sin(\pi k s)\cos\left[k\omega_0\left(t'-\frac{x}{c_k}\right)\right] \tag{31}$$

where, c_k is the propagation velocity of the frequency component $k\omega_0$ and t' is measured from a time when all frequencies are in phase. It follows that:

$$c_k=k\omega_0\Lambda/2\pi,\quad \text{or,}\quad 2\pi(c_k/c_0)\cdot(a/\Lambda_k)=ak\omega_0/c_0 \tag{32}$$

Using the dispersion relationship from Fig. 26 and Eq. (32), c_k can be determined for each discrete frequency. Figure 27 is a reproduction of the example provided by Follansbee and Frantz [53], where a trapezoidal pulse is dispersed through 0.61 m in a 4.6 mm bar. They also validated this example with experimental measurements and concluded that the bar dispersion corresponds to the mode one vibration, and described a Fourier transform methodology for dispersion correction.

The calculation of c_k from Bancroft's [10] or Davies's [5] tables is rather cumbersome. Gong *et al* [54] used a nonlinear curve fitting approach [56] to fit the dispersion relationships of the first mode of the vibration using an equation of the form:

$$\frac{c_k}{c_0}=A+\frac{B}{\left[C\left(\frac{a}{\Lambda_k}\right)^4+D\left(\frac{a}{\Lambda_k}\right)^3+E\left(\frac{a}{\Lambda_k}\right)^2+F\left(\frac{a}{\Lambda_k}\right)^{1.5}+1\right]} \tag{33}$$

where the constants A to F are fitting parameters.

Figure 28 shows Davies's [5] data for $\nu=0.29$, and that interpolated from Bancroft's [10] data. Both data are curve fitted to Eq. (33) and the fitting parameters are presented in Table I. Gong *et al* [54] stated that if the parameters of Eq.

Table 2. Nonlinear fitting parameters of Bancroft's dispersion data (boldface) and interpolated data (*Italic*)

	Fitting Parameters					
ν_B	A	B	C	D	E	F
0.20	**0.58750**	**0.41473**	**41.3050**	**12.2080**	**−9.4836**	**3.0893**
0.21	*0.58626*	*0.41589*	*38.7150*	*13.2570*	*−9.3202*	*3.0344*
0.22	*0.58499*	*0.41708*	*36.0510*	*14.3390*	*−9.1552*	*2.9774*
0.23	*0.58367*	*0.41832*	*33.3120*	*15.4580*	*−8.9934*	*2.9202*
0.24	*0.58232*	*0.41958*	*30.5640*	*16.5510*	*−8.8078*	*2.8552*
0.25	**0.58092**	**0.42088**	**27.7920**	**17.6360**	**−8.6088**	**2.7857**
0.26	*0.57972*	*0.42201*	*26.2570*	*18.0050*	*−8.2969*	*2.7116*
0.27	*0.57850*	*0.42315*	*24.6740*	*18.3850*	*−7.9743*	*2.6328*
0.28	*0.57724*	*0.42434*	*23.0390*	*18.7900*	*−7.6529*	*2.5538*
0.29	*0.57594*	*0.42555*	*21.3260*	*19.2240*	*−7.3258*	*2.4713*
0.30	**0.57460**	**0.42681**	**19.5300**	**19.7020**	**−7.0054**	**2.3897**
0.31	*0.57344*	*0.42790*	*18.6680*	*19.6640*	*−6.6213*	*2.3118*
0.32	*0.57228*	*0.42901*	*17.7810*	*19.6360*	*−6.2337*	*2.2327*
0.33	*0.57106*	*0.43016*	*16.7640*	*19.6790*	*−5.8543*	*2.1532*
0.34	*0.56983*	*0.43132*	*15.7410*	*19.7140*	*−5.4671*	*2.0717*
0.35	**0.56855**	**0.43254**	**14.6020**	**19.8090**	**−5.0851**	**1.9895**

(33) are known for a specific Poisson's Ratio, Eqs. (32) and (33) can be numerically solved to obtain the values of c_k for all discrete Fourier frequencies. The table provided by Bancroft contains data for Poisson's Ratio in the range 0.10 to 0.40 with an increment of 0.05 (Fig. 27). This data table is inadequate for intermediate Poisson's Ratios and interpolation is suggested. The nonlinear fitting parameters (Eq. 33) can then be obtained. Fitting parameters for these intermediate Poisson's Ratios are presented in Table II. With this background, a step-by-step method for dispersion correction is described next.

Dispersion correction methodology

In Hopkinson Bar experiments, the location of the strain gage is a certain distance away from the specimen-bar interfaces. The main objective of dispersion correction is to transform and reconstruct the strain gage signals from the location of their measurements back to the specimen-bar interface using Fourier transform and the dispersion equation, $c_k/c_0 = f(\nu, a/\Lambda)$. The method described by Li and Lambros [57] is followed, which is similar to the methods described by Follansbee and Frantz [53] and Gong *et al* [54].

Any arbitrary time function $f(t)$ can be expressed in terms of a Fourier series:

$$f(t) = \frac{A_0}{2} + \sum_{k=1,2,..}^{\infty} [A_k \cos(k\omega_0 t) + B_k \sin(k\omega_0 t)] \qquad (34)$$

In the case of a time function with $2N+1$ number of data points, as is the case of Hopkinson Bar signals, with a constant time interval of ΔT, Eq. (34) can be written as:

$$f(n\Delta T) = \frac{A_0}{2} + \sum_{k=1,2,..}^{N} [A_k \cos(k\omega_0 n\Delta T) + B_k \sin(k\omega_0 n\Delta T)] \qquad (35)$$

where, $n=1, 2, 3,..., 2N$; $k=1, 2, 3,..., N$; $\omega_0 = 2\pi/T = 2\pi/(2N\Delta T)$; and the Fourier coefficients are given by:

$$A_0 = \frac{2}{T} \cdot \int_0^T f(t) \cdot dt = \frac{2}{T} \cdot \sum_{n=1,2,..}^{2N} f(n\Delta T) \cdot \Delta T \qquad (36a)$$

$$A_k = \frac{2}{T} \cdot \int_0^T f(t)\cos(k\omega_0 t) \cdot dt = \frac{2}{T} \cdot \sum_{n=1,2,..}^{2N} f(n\Delta T)\cos(k\omega_0 n\Delta T) \cdot \Delta T \qquad (36b)$$

$$B_k = \frac{2}{T} \cdot \int_0^T f(t)\sin(k\omega_0 t) \cdot dt = \frac{2}{T} \cdot \sum_{n=1,2,..}^{2N} f(n\Delta T)\sin(k\omega_0 n\Delta T) \cdot \Delta T \qquad (36c)$$

As an example, consider Fig. 27. The trapezoidal time function $f(t)$ is described with 2001 data points, which corresponds to N=1000. The values of the corresponding Fourier coefficients, A_0, A_k, and B_k, computed using Eq. (36) are presented in Fig. 29. The coefficient $A_0 = 1.0$, B_ks are zero, and the values of A_ks for $k=2$, 4, and 6, are zero; which is the same as the analytical values given by Eq. (30).

The values of c_k/c_0 for a specific value of ν can be determined by numerically solving Equations (32) and (33) for each k. If the accurate value of c_0 is known, c_k can then be

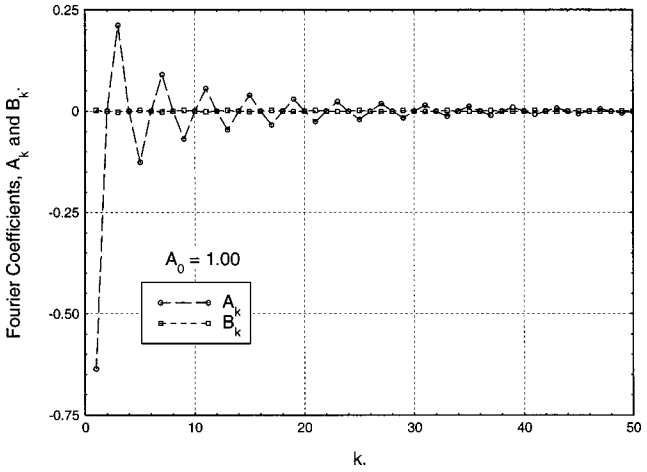

Fig. 29 The first 50 Fourier coefficients for a trapezoidal function

determined. With dispersion, a particular frequency component will travel with the phase velocity c_k, instead of c_0, and will travel a distance Δx in time $\Delta x/c_k$ instead of time $\Delta x/c_0$. The difference in the phase angle can be written as:

$$\phi = k\omega_0 \cdot [(\Delta x/c_k) - (\Delta x/c_0)] \tag{37}$$

where Δx is positive in forward, and negative in backward dispersion schemes, respectively. If one omits the part $\Delta x/c_0$ from Equation (37), it is possible to visualize that the time function $f(t)$ is traveling in x as well as in t [57].

$$\phi_{TS} = k\omega_0(\Delta x/c_k) \tag{38}$$

Reconstruction of a pulse with forward or backward dispersion is then obtained using the following transformation equation and using either ϕ or ϕ_{TS}.

$$F(n\Delta T) = \frac{A_0}{2} + \sum_{k=1,2,..}^{N} [A_k \cos(k\omega_0 n\Delta T - \phi) + B_k \sin(k\omega_0 n\Delta T - \phi)] \tag{39}$$

Figure 27 shows the forward dispersed trapezoidal pulse with symbols, while the solid line represents the original trapezoidal pulse. Following the same procedure, the dispersed signal can also be transformed and backward dispersed to recreate the trapezoidal pulse.

Figure 29 shows that the first fifty values of k contain the most information of constants A_k and B_k. A careful choice of the upper limit of k can significantly reduce the computational time. Li and Lambros [57] suggested the choice of the upper limit of k by using the Nyquist frequency ($f_N = 1/2\Delta t$: Δt—time interval between two consecutive sampling points) of the data acquisition system or measuring device.

Determination of c_0 and start point of Hopkinson Bar pulses

Lifshitz and Leber [31] identified that many researchers discussed the bar calibration, the determination of the starting point of strain pulses, and the determination of the bar velocity c_0 from the ''bars apart'' calibration experiments. However, no one has illustrated the methodology followed in determining the bar velocity. It is known that the bar velocity c_0 can be determined by the vibration method; however, Lifshitz and Leber [31] proposed an iterative dispersion correction method to determine the value of c_0, and showed that the shape of the dynamic stress-strain curve is very sensitive to small errors in the value of c_0 and to errors in shifting the pulses along the time axis.

In this method, a ''bars apart'' calibration experiment is conducted first. This gives a reflected pulse, which is almost identical to the incident pulse. A book value of c_0 is taken as the first approximation. The distance between the center of the strain gage and the free end of the bar (specimen end) Δx is measured. Two identical time windows of duration/period T are chosen with a time interval of $2\Delta x/c_0$ between them, such that the incident pulse is positioned inside the middle of the first time window and occupies about a 75% span in time. If the assumed value of c_0 is approximately correct, the reflected pulse will be positioned in the middle of the second time window.

A discrete Fourier transform of the incident pulse is performed to calculate the Fourier coefficients using Eq. (36). The dispersion correction methodology described earlier is then utilized to predict the reflected pulse using the phase angle ϕ_{TS}. This will place the dispersed incident pulse (predicted reflected pulse) on top of the negative of the reflected pulse. The predicted and measured reflected pulses are then compared for a good match. If a good match is not obtained, a new value of c_0 is assumed and the iterative procedure continued until a good match is obtained.

Once the correct value of c_0 is determined, dispersion correction and identification of the start point of the pulses of an actual experiment can proceed. A typical Hopkinson Bar experiment with a specimen produces incident, reflected, and transmitted pulses as a function of time $\varepsilon_I(t)$, $\varepsilon_R(t)$, and $\varepsilon_T(t)$, respectively. Generally, the distance between the strain gage on the incident bar and IB-S interface is denoted as $\Delta x = \Delta x_1$, and that of the S-TB interface and the strain gage on the transmitter bar are denoted as $\Delta x = \Delta x_2$. A time window of period T is first chosen for the incident pulse $\varepsilon_I(t)$, such that it is positioned inside the middle of the time window and occupies about a 75% span in time (Fig. 30).

The start point of the time window for the reflected pulse $\varepsilon_R(t)$ is then identified at a distance $2\Delta x_1/c_0$ away from the incident pulse window, and for the transmitted pulse $\varepsilon_T(t)$ at a distance[9] $\{(\Delta x_1 + \Delta x_2)/c_0\} + \tau_S$, where $\tau_S = H_S/c_S$ is the characteristic time of the specimen. Note that the values of c_0 used in these calculations are the values obtained from the procedure described above. After the identification of the start point of the time window for reflected and transmitted pulses with respect to the incident pulses, the dispersion correction methodology is applied.

The incident pulse is then forward dispersed by $\Delta x = \Delta x_1$; the reflected pulse is backward dispersion corrected by $\Delta x = -\Delta x_1$; and the transmitted pulse is backward dispersion corrected by $\Delta x = -\Delta x_2$. If the phase angle ϕ_{TS} is

[9]Lifshitz and Leber [31] neglected τ_s in this expression.

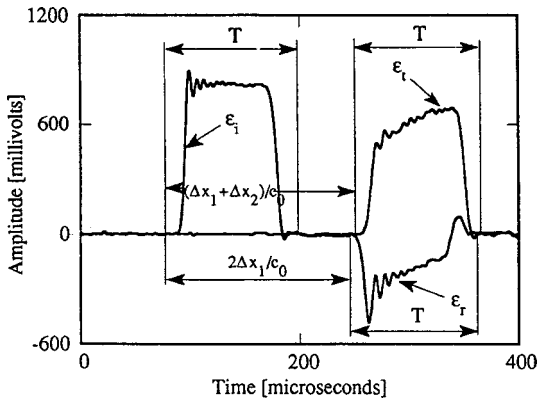

Fig. 30 Location of time windows for a dispersion calculation. Reproduced from [31], Fig. 4, p 729.

used in the dispersion correction, then all the pulses will be placed in a single time window, and thus identification of a start point becomes arbitrary. However, the transmitted pulse will show a time lag as compared to the incident and reflected pulses, which corresponds to the time required for stress homogenization in the specimen.

Zhao and Gary [32] proposed an iterative method of determining the start/beginning of strain/stress pulses, which involve 1D simulation of the experiment with fictitious linear elastic specimens to match the initial portion of the reflected and transmitted pulse, using the modulus of the specimen as the parameter. It is assumed that the shape of the pulse is more reliable and the materials tested remain elastic in the initial stages of deformation. Once a good match in the shape of the pulses between the simulation and experiment is obtained, the start point of experimental pulses can be identified because of the fact that the simulation results are known.

This method was criticized by Li and Lambros [57] and an alternate method was suggested. A sampling window of 200 data points are taken for the incident pulse, the slopes of the consecutive points are determined, and if 90% of the slopes are negative, the start of the time window is taken as the start time of the incident pulse. However, Li and Lambros did not explicitly mention how the start of the reflected and transmitted pulse was determined. This method is arbitrary and should be used with greater care.

Zhao and Gary [32,34] also solved the 1D inverse problem using any of the measured Hopkinson Bar responses as input and predicting the others, while assuming a material model for the specimen. The parameters of the material model are determined by trial and error, until a good match is obtained with the experimental data. The authors claimed that ''the chosen model, with the set of parameters which gives the best agreement with experimental data, can be considered as the representative model of the specimen. As a result, the stress and strain fields in the specimen are known so that a stress-strain curve is found. The assumption on the uniformity of stress and strain fields is then no longer needed in such a method. Furthermore, it is possible to give a stress-strain curve at a constant strain rate via the identified model.''

This method is the state-of-the art in small strain measurements using the Hopkinson Bar technique. Also, knowing that all practical finite diameter Hopkinson bars are dispersive in nature, a 1D analysis (radial inertia, radial expansion, and friction effects are neglected) with the assumed material model, may not provide realistic model parameters. With the help of dynamic explicit hydrocodes, 3D finite element analyses can be performed to simulate the Hopkinson Bar experiments, and thus the material behavior during SHPB testing can be back calculated from the material model input if a good match between simulation and experiment can be obtained.

Recent advances in unlimited strain measurement

The duration of the pulse length that can independently be measured in a traditional Hopkinson Bar experiment is governed by the length of the incident bar. The rule of thumb is that the pulse length produced in the incident bar is approximately double the length of the striker bar; and the maximum admissible striker bar length is less than one quarter of the striker bar. If this rule of thumb is followed, the incident pulse will be separated from the reflected pulse in time as recorded by the strain gages mounted on the bar (Fig. 25).

Park and Zhou [58] developed a method of separating the ascending and descending waves in the time domain (using the method of characteristics) through a one-point measurement. This method allows unlimited measurement of the strain in both the bars and is useful for large deformation experiments, eg, three-point bending, nonequilibrium crushing of the honeycomb, and foamed materials. Later, Zhao and Gary [33] developed a two-point measurement technique and combined the dispersion correction methodology in the unlimited duration of measurement by the same separation of waves principle described in [58]. This method is used by Zhao [59] in testing polymeric foams at high and medium strain rates, where the total nonequilibrium compression is obtained by repeated pulses from a single experiment.

A more general theory of ''an optimization method for separating and rebuilding 1D dispersive waves'' using *n*-point measurement was developed by Bussac *et al* [60]. Their generalized method can be used for single- and multipoint measurements for both elastic and visco-elastic bar materials. Because the analysis is performed in the frequency domain and the dispersion correction methodology is inherent in such a measurement technique, identification of zeros of the pulses can also be automatically performed using Lifshitz and Leber's [31] method.

Stress wave propagation in the specimen

The specimen used in a SHPB experiment may have a material property that is very different from that of the bars. In the analysis of the SHPB, the stress wave propagation in the specimen during dynamic deformation should be considered. In 1D analysis, Eqs. (15) and (16) provide the boundary conditions to be applied with constitutive material behavior of the specimen. Micunovic and Baltov [61] presented a detailed analysis of plastic wave propagation in the specimen and found that under the plastic deformation state of the specimen, the axial stress distribution in the specimen is steady and uniform. Following Micunovic and Baltov's [61] procedure, the analysis can be further extended to different families of materials, eg, linear and nonlinear visco-elastic specimens and specimens with memory effects.

SUMMARY

In most textbooks and articles on Split-Hopkinson Pressure Bar (SHPB) techniques, the pioneering work of Bertram Hopkinson (1914) [4], RM Davies (1948) [5], and H Kolsky (1949) [6] are cited without any detail of their specific contributions in the development of SHPB experimental technique. In this review, contributions from the above three classic papers are presented chronologically. Research and development on the SHPB experimental technique over the past 50 years since Kolsky's first introduction of this famous technique is presented. However, the emphasis is on the fun-

damental compression Split-Hopkinson technique. A step-by-step methodology of experimental design, data analysis, and recent developments are summarized.

Hopkinson Bar experimental techniques allow one to load a relatively small specimen ($H_S/D_B \approx 1.0$) under dynamic conditions, while 1D stress wave propagation theory and associated assumptions in long cylindrical rods are used to analyze the data recorded via strain gages mounted on the bars. One-dimensional analysis of Hopkinson Bar experimental data was first formulated by Kolsky in 1949, and is mostly followed in today's data analysis with some modifications. The main 1D assumptions of Hopkinson Bar technique are: i) the wave propagation in the bars is free of dispersion, ii) the effect of interface friction and inertia of the specimen is negligible, iii) the stress wave reverberation in the specimen is negligible, iv) the stress equilibrium in the specimen is achieved in π travel/characteristic time, and v) the specimen-bar interfaces remain planar at all time.

Since RM Davies (1948) [5] published his critical review on the original Hopkinson Pressure Bar technique, it is well documented in the literature that all the above mentioned 1D assumptions are subjected to criticism. Subsequently, researchers have had to provide enough proof that the above assumptions remain valid during their experiments. A critical review on the validity of 1D assumptions has been presented in this article following the critical review of RM Davies (1948) [5].

It has been discussed that finite diameter bars are prone to dispersion effects (assumption i) is thus not valid); however, methodologies following the solution of the Pochhammer (1876) [8] frequency equation are available to correct this problem. Conditions that minimize the effect of interface friction and inertia effects are generally used in the design of the specimen geometry (a methodology to validate assumption ii) Neglecting the stress wave reverberation in the specimen (assumption iii) simplifies the calculation of the bar-specimen interface velocities; however, they are not sufficient conditions for displacement and stress continuities in those interfaces. Higher order analysis, considering the displacement and stress continuity conditions at the bar-specimen interfaces, is identified as a future research topic.

The assumption of stress equilibrium in the specimen allows one to equate the forces in the bar-specimen interfaces, which further simplifies the determination of the strain rate of the specimen from the reflected pulse; and the average stress in the specimen from the transmitted pulse as a function of time. This assumption is usually validated by *1-wave* and *2-wave* analyses of experimental data.

The condition of stress equilibrium is also used in specimen design. Researchers from the ceramic community first identified that slow loading via a shaped pulse is an essential condition in testing brittle ceramics, which also provide an almost constant test strain rate for linear-elastic solids. The use of a ramp-shaped pulse allows for the calculation of stress nonequilibrium factor $R(t)$, considering the stress wave reverberation in the specimen, following the method of characteristics. This analysis showed that the initial nonequilibrium is as high as 200%; however, it exponentially decreases to about 10% in four reverberations in the specimen.

Following this analysis, and utilizing the linear relationship between particle velocity and stress (1D stress wave propagation theory), it was concluded that the dynamic deformation of specimens under SHPB loading conditions occurs under a non-equilibrium state of stress (assumption iv is thus not generally correct). Many research papers, including the first paper by Kolsky (1949) [6], mentioned the fact that the initial portion of the stress-strain plot is unreliable, which supports the condition of stress nonequilibrium discussed above. The stress non-equilibrium issues can be addressed by plotting stress-strain rate instead of stress-strain, and time-averaging the nonequilibrium stress and strain rate data using a time window not less than one characteristic time of the specimen.

The planar condition of the bar-specimen interface is technically valid for soft specimens; however, soft specimens have an inherent problem of poor transmission, which is generally addressed by the use of low-impedance bars or hollow transmission bars. The planar interface condition is generally not valid because the eigen-functions of a finite diameter bar possess high frequency modes, and these modes are a strong function of the end boundary conditions. A simple model of a hard specimen, with a diameter less than the bar, is presented to analyze nonplanar interface conditions. It has been inferred from the analysis of the nonplanar interface that the strain measured in such situations will be larger than reality. The violation of the planar bar-specimen interface is well known in the ceramic research community, where indentations in the bar edges are observed and the use of high hard ceramic loading blocks are common to address this issue. In conclusion, the strain measured from the integral of the reflected pulse will thus predict higher strain, which in turn will generate a lower modulus in the initial portion of the stress-strain diagram. A critical analysis of the validity of most assumptions in 1D Hopkinson Bar analysis is presented in this review paper.

In light of the validity of 1D Hopkinson bar assumptions, a step-by-step methodology of the Hopkinson Bar experiment is outlined. These steps are a) the calibration of the bars, b) the specimen design, c) the Hopkinson bar experiment, d) the dispersion correction, and e) the data representation. Accurate determination of the density ρ_B, Poisson's Ratio ν_B, and wave velocity c_0 of the bars is emphasized in the literature for correctness. Book values are found to produce significant inaccuracies.

''Bars apart'' calibration can be used in accordance with dispersion correction methodology to determine the bar velocity accurately, and strain correction factors (due to material non-homogeneity and attenuation) of the bars. ''Bars together'' calibration, on the other hand, provides a stress correction factor (imperfect contact, effect of lubrication, etc). Specimen design is discussed in the light of minimizing the friction, inertia, and stress non-equilibrium. A good experiment is one where the bars and specimens possess high dimensional tolerances, the bars are aligned accurately, and the bearing/support frictions are minimum. Dispersion cor-

rection of bar signals is mandatory, and the state-of-the-art methodology is described in detail. Inadequacy of nonlinear fitting parameters of Bancroft's dispersion data is compensated by providing parameters for a 0.01 increment in Poisson's Ratio in the range $0.20 \leqslant \nu_B \leqslant 0.35$ by interpolating and curve-fitting Bancroft's tabulated data.

The determination of an accurate longitudinal wave speed of the bar c_0 using the ''bars apart'' calibration experiment and dispersion correction in the frequency domain is outlined, where the delay setting of individual signals are inherent to the process. Because of the accurate delay setting of individual signals through dispersion correction methodology, the data representation in *1-wave*, *2-wave*, and *3-wave* analysis is found through straight-forward algebraic operations.

In addition to the classic Hopkinson Bar experimental technique, and the step-by-step procedures described, the state-of-the-art in Hopkinson Bar techniques is summarized. These include split techniques in tension, shear, torsion, combined loading, multi-axial loading, dynamic recovery experiments using momentum trapping devices, pulse shaping, and unlimited strain measurement techniques. The history of Hopkinson Bar development together with the discussion of major developments in the 20th century makes this review on Hopkinson Bar experimental techniques complete.

ACKNOWLEDGMENT

This article is prepared through participation in the Composite Materials Technology (CMT) Collaborative Program sponsored by the US Army Research Laboratory under Cooperative Agreement DAAD09-01-2-0005.

REFERENCES

[1] Hopkinson J (1901), On the rupture of iron wire by a blow (1872), Article 38, *Original Papers-by the late John Hopkinson, Vol II, Scientific Papers*, B Hopkinson (ed), Cambridge Univ Press, 316–320.
[2] Hopkinson J (1901), Further experiments on the rupture of iron wire (1872), Article 39, *Original Papers-by the late John Hopkison, Vol II, Scientific Papers*, B Hopkinson (ed), Cambridge Univ Press, 316–320.
[3] Hopkinson B (1904–1905), The Effects of Momentary Stresses in Metals, *Proc. R. Soc. London, Ser. A* **74**, 498–506.
[4] Hopkinson B (1914), A method of measuring the pressure produced in the detonation of high explosives or by the impact of bullets, *Philos. Trans. R. Soc. London, Ser. A* **213**, 437–456.
[5] Davies RM (1948), A critical study of the Hopkinson pressure bar, *Philos. Trans. R. Soc. London, Ser. A* **240**(821), 375–457.
[6] Kolsky H (1949), An investigation of the mechanical properties of materials at very high rates of loading, *Proc. Phys. Soc. London, Sect. B* **62**(II-B), 676–700.
[7] Love AEH (1934) *Mathematical Theory of Elasticity, 2nd edition*, Cambridge Univ Press.
[8] Pochhammer L (1876), Uber Fortplanzungsgeschwindigkeiten kleiner Schwingungen in einem unbergrenzten isotropen Kreiszylinder, *J. Reine Angew. Math.* **81**, 324 (German).
[9] Chree C (1889), The equations of an isotropic elastic solid in polar and cylindrical coordinates, their solution and applications, *Trans. Cambridge Philos. Soc.* **14**, 251–369.
[10] Bancroft D (1941), The velocity of longitudinal wave in cylindrical bars, *Phys. Rev.* **59**, 588–593.
[11] Boltzmann L (1876), *Pogg Ann Erg* **7**, 624.
[12] Taylor GI (1946), *J Instn Civ Engrs* **8**, 486.
[13] ASM Int (2000), *ASM Handbook* Vol 8, Mechanical Testing and Evaluation, ASM Int, Materials Park OH, 462–476.
[14] Gray III GT (2000), Classic split-Hopkinson pressure bar testing, *ASM Handbook* Vol 8, Mechanical Testing and Evaluation, ASM Int, Materials Park OH, 462–476.
[15] Graff KF (1975), *Wave Motions in Elastic Media*, Oxford Univ Press, Dover Publ Inc New York.
[16] Meyers MA (1994), *Dynamic Behavior of Materials*, John Wiley & Sons, Inc.
[17] Nemat-Nasser S (2000), Introduction to high strain rate testing, *ASM Handbook* Vol 8, Mechanical Testing and Evaluation, ASM Int, Materials Park OH, 427–428.
[18] ASM Int (2000), High strain rate tension and compression test, *ASM Handbook*, Vol 8, Mechanical Testing and Evaluation, ASM Int, Materials Park OH, 429–446.
[19] Lindholm US and Yeakley LM (1968), High strain rate testing: Tension and compression, *Exp. Mech.* **8**, 1–9.
[20] Nicholas T (1980), Tensile testing of materials at high rates of strain, *Exp. Mech.* **21**, 177–185.
[21] Harding J and Huddart J (1979), The use of the double-notch shear test in determining the mechanical properties of uranium at very high rates of strain, *Proc of 2nd Int Conf Mechanical Properties at High Rates of Strain*, J Harding (ed), Inst of Physics, London, 49–61.
[22] Ferguson WG, Hauser JE, and Dorn JE (1967), The dynamic punching of metals, dislocation damping in zinc single crystals, *Br. J. Appl. Phys.* **18**, 411–417.
[23] ASM Int (2000), High strain rate shear testing, *ASM Handbook*, Vol 8, Mechanical Testing and Evaluation, ASM Int, Materials Park OH, 447–461.
[24] Gilat A (2000), Torsional Kolsky bar testing, *ASM Handbook*, Vol 8, Mechanical Testing and Evaluation, ASM Int, Materials Park OH, 505–515.
[25] Nemat-Nasser S (2000) Recovery Hopkinson bar techniques, *ASM Handbook*, Vol 8, Mechanical Testing and Evaluation, ASM Int, Materials Park OH, 477–487.
[26] Nemat-Nasser S, Isaacs J, and Rome J 2000, Triaxial Hopkinson techniques, *ASM Handbook*, Vol 8, Mechanical Testing and Evaluation, ASM Int, Materials Park OH, 516–518.
[27] Davies EDH and Hunter SC (1963), The dynamic compression test of solids by the method of the split Hopkinson pressure bar (SHPB), *J. Mech. Phys. Solids* **11**, 155–179.
[28] Gama BA, Gillespie Jr JW, Mahfuz H, Raines RP, Haque A, Jeelani S, Bogetti TA, and Fink BK (2001), High strain-rate behavior of plain-weave S-2 glass/vinyl ester composites, *J. Compos. Mater.* **35**(13), 1201–1228.
[29] Gray III GT (2000), Split-Hopkinson pressure bar testing of soft materials, *ASM Handbook*, Vol 8, Mechanical Testing and Evaluation, ASM Int, Materials Park OH, 488–496.
[30] Subhash G and Ravichandran G (2000), Split-Hopkinson pressure bar testing of caramics, *ASM Handbook*, Vol 8, Mechanical Testing and Evaluation, ASM Int, Materials Park OH, 488–496.
[31] Lifshitz JM and Leber H (1994), Data processing in the split Hopkinson pressure bar tests, *Int. J. Impact Eng.* **15**(6), 723–733.
[32] Zhao H and Gary G (1996), On the use of SHPB techniques to determine the dynamic behavior of materials in the range of small strains, *Int. J. Solids Struct.* **33**(23), 3363–3375.
[33] Zhao H and Gary G (1997), A new method for the separation of waves: Application to the SHPB technique for an unlimited duration of measurement, *J. Mech. Phys. Solids* **45**(7), 1185–1202.
[34] Zhao H (1998), A study on testing techniques for concrete-like materials under compressive impact loading, *Cem. Concr. Compos.* **20**, 293–299.
[35] Davies EDH and Hunter SC (1963), The dynamic compression testing of solids by the method of split Hopkinson pressure bar (SHPB), *J. Mech. Phys. Solids* **11**, 155–179.
[36] Gorham DA, Pope PH, and Cox O (1984), Sources of error in very high strain rate compression tests, *Inst. Phys. Conf. Ser.* **70**, 151–158.
[37] Follansbee PS (1995), The Hopkinson bar, Mechanical Testing, *ASM Handbook*, ASM Int, 198–203.
[38] Tracy CA (1987), A compression test for high strength ceramics, *J. Test. Eval.* **15**, 393–396.
[39] Couque C, Albertini C, and Lankford J (1993), Failure mechanism in a uni-directional fiber-reinforced thermoplastic composite under uniaxial, in-plane biaxial and hydrostatically confined compression, *J. Mater. Sci. Lett.* **12**, 1953–1957.
[40] Gray III GT, Idar DJ, Bluementhal WR, Cady CM, and Peterson PD (2000), High- and low-strain rate compression properties of several energetic material composites as a function of strain rate and temperature, *11th Detonation Symposium*, Snow Mass CO, J Short (ed), Amperstand Publ.
[41] Field JE, Walley SM, Bourne NK, and Huntley JM (1998), Review of experimental techniques for high rate deformation studies, *Proc Acoustics and Vibration Asia '98*, Singapore, 9–38.
[42] Gray III GT, Bluementhal WR, Trujillo CP, and Carpenter II RW

(1997), Influence of temperature and strain rate on the mechanical behavior of Adiprene L-100, *J Phys (France) IV Colloq, C3* (EURODYMAT 97), **7**, 523–528.
[43] Gary G, Klepaczko JR, and Zhao H (1995), Generalization of split Hopkinson bar technique to use visco elastic materials, *Int. J. Impact Eng.* **16**, 529–530.
[44] Gary G, Rota L, and Zhao H (1996), Testing viscous soft materials at medium and strain rates, *Constitutive Relation in High/Very High Strain Rates*, K Kawata and J Shioiri (eds), Springer-Verlag, Tokyo, 25–32.
[45] Chen W, Zhang B, and Forrestal MJ (1999), A split Hopkinson bar technique for low impedance materials, *Exp. Mech.* **39**, 1–5.
[46] Nemat-Nasser S, Issacs JB, and Starrett JE (1991), Hopkinson techniques for dynamic recovery experiments, *Proc. R. Soc. London Ser. A* **453**, 371–391.
[47] Anderson C, O'Donoghue P, Lankford J, and Walker J (1992), Numerical simulations of SHPB experiments for the dynamic compressive strength and failure of ceramics, *Int. J. Fract.* **55**, 193–208.
[48] Cosculluela A, Cagnoux J, and Collombet F (1991), Two types of experiments for studying uniaxial dynamic compression of alumina, *Shock Compression of Condensed Matter*, SC Schmidt, RD Dick, JW Forbes, and DG Tasker (eds), Elsevier Science Pub, 951–954.
[49] Blumenthal WR (1992), High strain rate compression and fracture of B4C-aluminum cermets, *shock-wave and high strain rate phenomena in materials*, MA Meyers, LE Muri, and KP Staudhmmer (eds), Marcel Dekker, 1093–1100.
[50] Ravichandran G and Subhash G (1994), Critical appraisal of limiting strain rates for compression testing of ceramics in a split-Hopkinson pressure bar, *J. Am. Ceram. Soc.* **77**, 263–267.
[51] Chen W, Subhash G, and Ravichandran G (1994), Evaluation of ceramic specimen geometries used in split Hopkinson pressure bar, *Dymat* **1**, 191–210.
[52] Ravichandran G (2002), Personal communication, Oct.
[53] Follansbee PS and Frantz C (1983), Wave propagation in the split Hopkinson pressure bar, *ASME J. Eng. Mater. Technol.* **105**, 61–66.
[54] Gong JC, Malvern LE, and Jenkins DA (1990), Dispersion investigation in the split Hopkinson pressure bar, *ASME J. Eng. Mater. Technol.* **112**, 309–314.
[55] Yew EH and Chen CS (1978), Experimental study of dispersive waves in beam and rod using FFT, *ASME J. Appl. Mech.* **45**, 375–457.
[56] Felice CW (May 1996), The response of soil to impulse loads using the split Hopkinson pressure bar technique, AFWL-TR-85-92, Final Report, Air Force Weapons Lab, Kirtland Air Force Base, NM.
[57] Li Z and Lambros J (1999), Determination of the dynamic response of brittle composites by the use of split Hopkinson pressure bar, *Compos. Sci. Technol.* **59**, 1097–1107.
[58] Park SW and Zhou M (1999), Separation of elastic waves in split Hopkinson bars using one-point strain measurements, *Exp. Mech.* **39**(4), 287–294.
[59] Zhao H (1997), Testing of polymeric foams at high and medium strain rates, *Polym. Test.* **16**, 507–516.
[60] Bussac M-N, Collet P, Gary G, and Othman R (2002), An optimization method for separating and rebuilding one-dimensional dispersive waves from multi-point measurements: Application to elastic or viscoelastic bars, *J. Mech. Phys. Solids* **50**, 321–349.
[61] Micunovic M and Baltov A (2002), Plastic wave propagation in Hopkinson bar-revisited, *Arch. Mech.* **54**(5–6), 577–602, Warszawa.

Bazle A Gama *received BS and MS degrees in Mechanical Engineering from the Bangladesh University of Engineering and Technology (BUET) where he served as a Lecturer and Assistant Professor from 1992 to 1995. His primary interest in computational mechanics inspired him to come to the United States to pursue graduate studies. In 1997, he completed a MS degree from Tuskegee University, Alabama, and started his PhD research in the Materials Science and Engineering Department at the University of Delaware. Since October 2000, he has been a full-time Research Professional at the University of Delaware Center for Composite Materials (UD-CCM). His major research interests are: composite mechanics, impact dynamics, and computational mechanics. He is a member of ASME, SAMPE, and SAE. This review paper was prepared as a part of his PhD dissertation focused on the development of new analytical and experimental Hopkinson Bar techniques.*

Sergey L. Lopatnikov *received his PhD in Physics and Mathematics from the Institute of Terrestrial Magnetism, Ionosphere, and Radiowave Propagation of the Russian Academy of Sciences in Moscow, Russia in 1977. He was also the organizer and first Director of the Laboratory of Mathematical Modeling in the ALL-Union Research Institute of Nuclear Geophysics and Geochemistry in Moscow. From 1989 to 1991, he was the official expert for the Environmental Committee of the Supreme Council of the USSR. From 1994 to 2000, Lopatnikov was the leading Research Scientist at Moscow State University, Department of Chemistry, and advisor to the Vice-Chairman of the Defense Committee of the Federal Council of the Russian Federation. He is currently a Distinguished Visiting Professor and Senior Scientist at the University of Delaware Center for Composite Materials (UD-CCM) where he conducts research on Split-Hopkinson Pressure Bar theory, shock impact behavior of porous materials, and attenuation of waves in fluid-filled permeable poro-elastic media. The author of more then 100 papers and two monographs, his scientific interests include the physics of weak and strong wave propagation (particularly the acoustics of porous and random materials), the physics of liquid crystals, quantum mechanics, and physical chemistry.*

John W. Gillespie, Jr. *received his PhD in Mechanical and Aerospace Engineering from the University of Delaware in 1985. He holds a joint professorship in the Departments of Civil and Environmental Engineering and Materials Science and Engineering at the University of Delaware. As the current Director of the University of Delaware's Center for Composite Materials, he leads a successful University/Industry Consortium of 32 members in the commercialization of composites science technology. Since 1998, he has served as a member on the National Research Council's Board on Manufacturing and Engineering Design (BMAED) as well as serving as Chair of the National Research Council's National Materials Advisory Board Committee on High-Performance Structural Fibers for Advanced Polymer-Matrix Composites from 1999 to 2002. He received the Year 2000 J.H. "Judd" Hall Composites Manufacturing Award from the Society of Manufacturing Engineers (SME). He was also the co-recipient of the U.S. Army's Paul A. Siple Memorial Award for his research on multifunctional armor. He is the principal or co-principal on six issued patents with six patents pending and is the author of 10 books or book chapters, in addition to over 400 publications in refereed journals, conference proceedings, invited presentations, and reports.*